Input Areas to Mouse Visual Cortex and Role of Striatum in Cortical Plasticity

Inauguraldissertation

zur

Erlangung der Würde einer Doktorin der Philosophie

vorgelegt der

Philosophisch-Naturwissenschaftlichen Fakultät

der Universität Basel

von

Marina Moric

aus Kroatien

Basel, 2020

Genehmigt von der Philosophisch-Naturwissenschaftlichen Fakultät

auf Antrag von:

Dr. Georg Keller (Erstbetreuer)

Prof. Dr. Andreas Lüthi (Zweitbetreuer)

Prof. Dr. Valerio Mante (Externer Experte)

Basel, 13.10.2020

Prof. Dr. Martin Spiess (Dekan)

ACKNOWLEDGEMENTS

I would like to thank Georg Keller, who kindly gave me the opportunity to work with him. His advice, guidance and continuous support were instrumental in my professional and personal growth. To all the past and current lab members – thank you for the great ideas and discussions during lunches, coffee breaks, lab meetings and social occasions. Moreover, I would like to thank the members of my thesis committee – Andreas Lüthi, Tania Rinaldi Barkat and Valerio Mante for their support and valuable input.

Moreover, I am extremely grateful that Georg Keller, Matthias Heindorf, Marcus Leinweber, Aris Fiser, Felix Widmer and Baba Yogesh continuously answered my sometimes naïve questions about coding in MATLAB – without you, I would not progress to the point where I am today. Daniela Gerosa, Tingjia Lu and Elida Keller that were always ready to provide support. As researchers at the FMI, we are supported by excellent facilities, especially IT that resolves all issues with patience and ease. Thank you!

I am lucky to have family and friends that encouraged me to pursue my dream. Thank you for reading my applications, giving me suggestions, making me laugh, believing in me more than I do, and not letting the distance influence our bond. Special thanks to Sanja, Kreso, Barbara, Maja, Dunja, Luka, and Viki!

Finally, I am eternally grateful for meeting Martin Theiler, my partner, who keeps surprising me with his kindness. I am looking forward to our future adventures.

Thank you all!

For my grandmother Jelica and grandfather Milan who encouraged me to ask questions.

CONTENTS

PROLOGUE

When we learn a new skill, such as riding a bike, the brain learns the sequence of muscle commands needed to complete the task as well as sensory input that will be produced as a consequence of the behavior. For example, if we rotate the pedal with the intention to ride forward using the correct motor commands, the visual flow will be moving backward. The sequence of muscle contractions and subsequent sensory input will be used to create the internal model of riding a bike. This internal model will allow us to predict events based on the information presented by our sensory organs. Thus, if the visual flow unexpectedly moves sideways although we intended to move forward, the brain will signal deviation of the predicted stimuli. This prediction error will result in immediate adjustment of the motor commands that will, in some cases, prevent us from losing balance. In addition, the brain can use this information to adjust the behavior in the future and, eventually, we will effortlessly drive the bike.

Predictive processing framework of cortical function

Predictive processing theory of cortical computations was first proposed by von Helmholtz (Helmholtz, 1867) and postulates that, through sensorimotor experience, the brain generates an internal model of the world. This internal representation is used to compute predictions of the incoming sensory input based on the animal's behavior and compare it with input from sensory organs. Detected deviations from predicted input can be used to improve the internal representation, and/or evoke immediate motor response depending on the behavioral state (for review see (Keller and Mrsic-Flogel, 2018)). Through experience, the brain learns to perceive the environment by finding the internal model which minimizes the prediction errors and allow for more accurate interpretation of the sensory input.

Deviations, or prediction errors, can be positive or negative depending on the difference between the prediction (feedback or bottom-up input) and input from the sensory organs (feedforward or top-down input). If feedforward connection signals more than feedback connection (more input than predicted), positive prediction error neurons fire and activate internal representation neurons and feedback neurons, which in turn inhibits the positive prediction. If the feedforward input is lower than feedforward (less input than predicted), the opposite happens. The negative prediction error neurons

inhibit internal representation neurons and feedback neurons, thus inhibiting activity of negative prediction neurons (**Figure 1.1**).

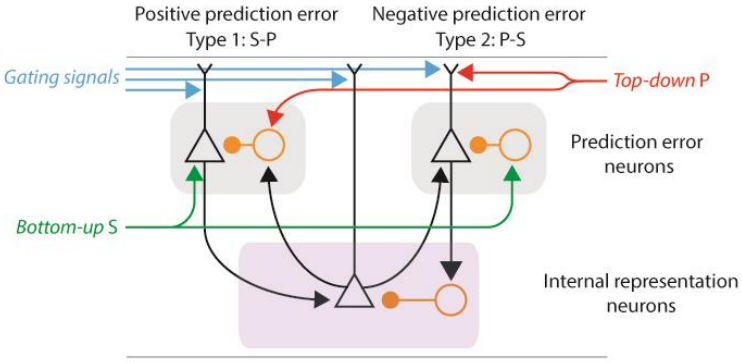

Figure 1.1. Schematic of the canonical circuit for predictive processing assuming hierarchical processing.
Black triangles represent excitatory whereas orange circles inhibitory neurons. Deviation between top-down (P, prediction) and bottom-up (S, sensory input) result in positive or negative prediction errors, encoded by Type 1 and Type 2 neurons, respectively. Adapted from: (Keller and Mrsic-Flogel, 2018).

In experimental settings, predictive processing principles are tested by creating perturbations of the generated sensory feedback. The visual system is a viable candidate to study predictive coding as locomotion is always followed by changes in the visual flow, and perturbations of the expected visual flow can easily be done in the virtual environment. Previous work of Dr. Keller and colleagues described negative visuomotor prediction error neurons in layer 2/3 of mouse visual cortex (Fiser et al., 2016; Keller et al., 2012; Zmarz and Keller, 2016) which are learned with experience (Attinger et al., 2017). Moreover, the area of anterior cingulate cortex and adjacent secondary motor cortex (A24b/M2) has been proposed as the source of visuomotor prediction in V1 (Fiser et al., 2016; Leinweber et al., 2017). This long-range cortical connection between V1 and A24b/M2 is shaped by visuomotor experience (Leinweber et al., 2017), and it has been speculated that its plasticity is driven by visuomotor prediction errors. Long-range connections needed for sensorimotor learning and perception of novel sensory input can be formed beyond developmental critical windows in which long-range cortical circuitry is reshaped (Darian-Smith and Gilbert, 1994; Gilbert and Li, 2012; Keck et al., 2008; Yamahachi et al., 2009). However, the specific mechanism in which formation of this long-range connection is being gated is still unclear. One of the candidates for gating the formation of long-range cortical connections are basal ganglia circuits.

Basal ganglia circuits

The basal ganglia are a set of interconnected subcortical nuclei which form a network with cortex and thalamus. Their anatomy and connectivity are evolutionary conserved across most vertebrates (Reiner et al., 1998; Stephenson-Jones et al., 2012). The basal ganglia have been implicated in action selection and organization of motor actions (Bar-Gad et al., 2003; Cui et al., 2013; Graybiel, 1998; Hikosaka et al., 2000; Kravitz et al., 2010; Markowitz et al., 2018; Mink, 1996), habit formation (Smith and Graybiel, 2013) and perceptual decision making (Wang et al., 2018; Znamenskiy et al., 2018). However, much of the ongoing interest in these nuclei derives from their role in human motor diseases such as dystonia, Huntington's and Parkinson's disease (for review see: (Nelson and Kreitzer, 2014)), as well as psychiatric disorders such as anxiety, substance use and eating disorders, major depression and schizophrenia (for review see: (Peters et al., 2016)).

Classically, basal ganglia circuits start with the unidirectional excitatory connection from the cortex to the striatum. Striatal projection neurons, modulated by dopamine, follow direct or indirect pathways, facilitated by D1 and D2 receptors, respectively. Striatal output from neurons that express D1 dopamine receptors project directly to internal globus pallidus/substantia nigra pars reticulata (GPi/SNr). These two inhibitory relays achieve the effect of a positive feedback to the cortex through disinhibition of the thalamus. In the indirect pathway, striatal neurons that express D2 dopamine receptors project to external globus pallidus (GPe) and disinhibit glutamatergic subthalamic nucleus (STN). STN in turn excites GPi/SNr and suppresses the thalamus, thus providing negative feedback to the cortex. Importantly, resulting input from thalamus innervates the original source of the cortical connection with striatum, thus closing the loop. This classical view of the basal ganglia network is improved through additional circuit elements: (1) second limb of the indirect pathway – a direct projection from GPe to GPi/SNr which enhances excitation of GPi/SNr; (2) hyperdirect pathway – a direct connection from cortex onto STN which results in more immediate suppression of the thalamus; (3) reciprocal connection between GPe and STN which can form negative feedback to terminate or modulate restraint by hyperdirect pathway (for a review see: (Shipp, 2017)) (**Figure 1.2**).

Dopaminergic neurons are thought to improve learning about reward and habit formation through reward and movement prediction errors (Bogacz, 2020). In striatum, dopamine is thought to influence

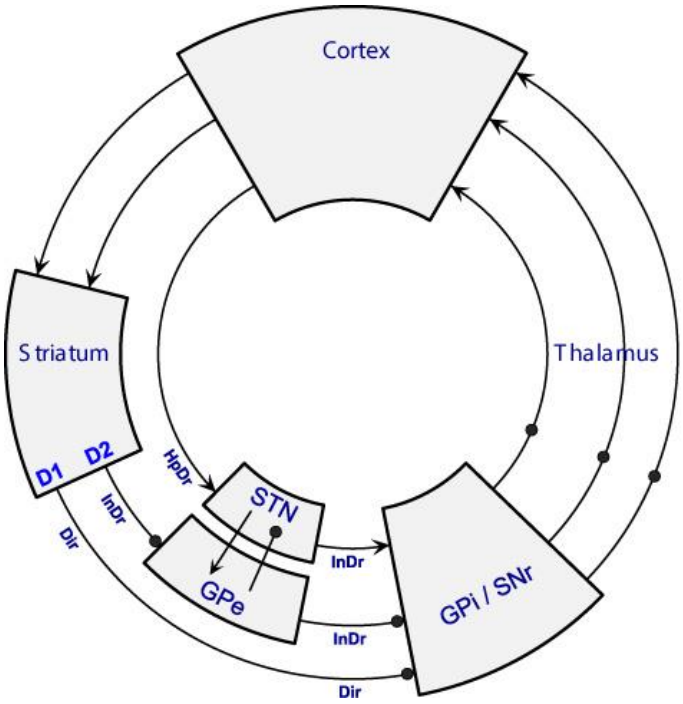

Figure 1.2. Classic direct and indirect pathway model of basal ganglia circuits with added circuit elements.
Whereas activity of the direct pathway disinhibits thalamus and provide positive feedback to the cortex, both indirect and hyperdirect pathways result in suppression of thalamic activity and serve as a negative feedback to the cortex. Arrowhead ending represents excitatory, whereas circle represents inhibitory connections. Abbreviations: Dir – direct pathway, InDr – indirect pathway, HprDr – hyper direct pathway, GPe – external globus pallidus, STN – subthalamic nucleus, GPi/SNr – internal globus pallidus/substantia nigra pars reticulata, D1 – dopamine D1 receptors, D2 – dopamine D2 receptors. Adapted from: (Shipp, 2017).

goal directed behavior by mediating reinforcement or aversion (Gremel and Costa, 2013) through interactions in the local circuitry (for review see (Burke et al., 2017)). Striatal neurons expressing D1 and D2 receptors differ in both their morphology and functionality (Gagnon et al., 2017; Keeler et al., 2014). Positive reinforcement strengthens while negative reinforcement weakens the response of neurons expressing D1 dopamine receptor; whereas opposite is the case for neurons expressing D2 dopamine receptor: positive and negative reinforcement is thought to weaken or strengthen their response, respectively (Schultz, 2013; Shin et al., 2018). Moreover, phasic activation of D1 and D2 receptors promotes long term potentiation and depression of glutamatergic synapses in neurons of direct and indirect pathways, respectively. This plasticity is modulated by previous experience (Paille et al., 2013; Shen et al., 2008).

Lesion studies in rodents have shown that many aspects of initial sensorimotor learning are conveyed through dorsomedial striatum (DMS), while execution of the behavior depends on the dorsolateral part of the striatum (DLS) (Castañé Anna et al., 2010; Hilario et al., 2012; Mink, 1996; Moussa et al.,

2011; Yin, 2010). However, although DMS decreases its activity when the behavior is learned, it has been shown that coordinated activity of both DMS and DLS is necessary to regulate movement initiation and execution (Ragozzino et al., 2002; Tecuapetla et al., 2016). Recent study has shown that DMS is needed to learn encoding cortical activity patterns that leads to positive outcome (Neely et al., 2018). Researchers used brain-machine interfaces to reinforce patterns of neural activity in the primary visual cortex of mice and rats. Animals, experiencing no visual input, were led by auditory stimuli to encode specific activity patterns in the primary visual cortex. Using optogenetic inhibition in DMS or DLS, researchers demonstrated that DMS is needed to learn the right sequence of neuronal activity, whereas inhibition of DLS did not affect learning. Moreover, DMS is considered to be involved in sensorimotor integration (Reig and Silberberg, 2014).

Speculation that the prediction error signals are passed through basal ganglia circuits to instruct plasticity between cortical areas involved in sensorimotor learning is based on findings in the songbirds. Zebra finches learn their songs by imitating tutor song and use auditory feedback to refine their vocalizations (Brainard and Doupe, 2000). The song system consists of two main pathways, with connectivity patterns as follows (for review see (Murphy et al., 2017)):

(1) Song motor pathway: HVC (analogous to premotor cortex) → RA (robust nucleus of the arcopallium, analogous to vocal regions of the primary motor cortex) → motor and premotor neurons of the brainstem → vocal and respiration muscles;

(2) Anterior forebrain pathway (AFP, homologous to basal ganglia circuits): HVC → area X (basal ganglia structure) → DLM (thalamic nucleus) → LMAN (lateral magnocellular nucleus of the anterior nidopallium, forebrain nucleus) → RA.

Neurons in HVC and RA are thought to encode for timing and specific vocalizations of the song, respectively (Hahnloser et al., 2002). During vocal learning, prediction errors between intended and produced vocalizations induce response in the auditory areas of the avian pallium (Keller and Hahnloser, 2009). Errors are speculated to shape neural circuitry between HVC and RA through activation of the AFP to allow precise timing of vocalizations (Luo et al., 2001). Importantly, lesions in any segment of the AFP prevent normal production of the song only if administered before the song has been learned and otherwise have no impact on song production (Ölveczky et al., 2005).

Aim of this thesis

Our brains allow us to perceive the outside world and learn to predict the consequences of actions through experience. Learning to predict the sensory input based on input from another sensory modality requires communication between respective cortical areas, as well as gating mechanisms which allow this connection to be formed. The aim of this thesis was to further expand our understanding of connectivity patterns within the visual cortex, as well as how formation of long-range cortical connections is gated.

Chapter 1 of this thesis aims to gain insight into the connectivity patterns of specific subsets of genetically identified cell types in the visual cortex. In addition, we asked if distinct types of source areas demonstrate particular connectivity distribution. This work was done in collaboration with Marcus Leinweber and Jan M. Sobczak.

Chapter 2 of this thesis provides preliminary data for visuomotor processing of striatum, input structure of basal ganglia, which have been speculated to gate the formation of long-range cortical connections.

CHAPTER 1: CELL-TYPE SPECIFIC BRAIN-WIDE INPUT TO MOUSE VISUAL CORTEX

This chapter is based on a non-published manuscript, a revised version will be submitted to a peer-reviewed journal in the future. The text and figures of this chapter correspond largely to the manuscript, with minor adaptations to formatting and numbering to conform to the style of this thesis.

Marcus Leinweber[1,3], Jan M. Sobczak[1,3], Marina Moric[1,2,3] & Georg B. Keller[1,2,4]
[1]Friedrich Miescher Institute for Biomedical Research, Basel, Switzerland
[2]Faculty of Natural Sciences, University of Basel, Basel, Switzerland
[3]These authors contributed equally
[4]Lead contact: georg.keller@fmi.ch

Primary visual cortex (V1) receives inputs from a distributed network of brain areas. Many of these projections are known to exhibit markedly different axonal termination patterns in V1. Whether these long-range inputs target specific subsets of genetically identified cell types in the visual cortex, and whether there is a systematic relationship between the type of source area and the pattern of genetically identified neurons, is still unclear. Here we characterize the brain-wide distribution of input to genetically identified populations of neurons using rabies tracing from V1 in different mouse lines that express Cre in subsets of excitatory or inhibitory neurons. We found that all starter neuron populations receive input from a large network of brain areas, with the vast majority (90%) of labelled neurons found in the cortex. Overall, the distribution of labelled cells was surprisingly similar for all starter neuron populations. Comparing innervation patterns across all starter neuron populations, however, we found systematic shifts from a strongly divergent bottom-up thalamic pattern to a parallel top-down, long-range cortical pattern. Notably, the innervation pattern of input originating in V1 itself more closely resembled the bottom-up input from thalamus than other cortical input.

Introduction

Neocortex is organized in six horizontal layers with functional units that span vertically through the layers referred to as cortical columns (Mountcastle, 1957). This columnar organization has long been interpreted as a sign of the existence of a repeated computational unit with a stereotypical circuit motif, often referred to as a canonical microcircuit (Douglas and Martin, 1991; Douglas et al., 1989). Differences between cortical areas are then interpreted as variations on a common motif (da Costa and Martin, 2010; Douglas and Martin, 1991; Douglas et al., 1989; Gilbert and Wiesel, 1979; Harris and Shepherd, 2015; Mountcastle, 1997). In the visual cortex, the structure of the local connectivity is well characterized (Van Hooser, 2007; Niell, 2015; Pfeffer et al., 2013; Xu et al., 2016). The main

feedforward drive of the circuit is the sensory information from the retina relayed through the lateral geniculate nucleus (LGN). However, these feedforward connections form less than 10% of synapses in visual cortex (da Costa and Martin, 2009; Da Costa and Martin, 2011), with majority of connections formed internally in the visual cortex and through inter-areal network with other brain areas (Wang and Burkhalter, 2007). Although cortical connectivity is complex, there appears to be a general structure by which afferents and efferents to and from a given cortical area are organized. The canonical model of a feedforward projection is an output connection to layer 4 (L4). In primary sensory areas of the cortex, the main source of this projection is the thalamus. L4 projects to layer 2/3 (L2/3), and from there signals propagate to deeper layers (L5 and L6), which, in turn, project to subcortical structures such as basal ganglia, the colliculus, and the spinal cord (Baker et al., 2018; Callaway, 2004; Douglas and Martin, 2004; Gerfen et al., 2018; Gilbert and Wiesel, 1979; Harris and Shepherd, 2015). In addition to the thalamic projection to L4, there is a parallel projection to infragranular layers (Constantinople and Bruno, 2013; Denardo et al., 2015; Douglas and Martin, 1991; Freund et al., 1989; Quiquempoix et al., 2018). Recurrent connections exist within layers, but these are more common in L2/3 than in other layers (Douglas and Martin, 2004).

Inhibitory interneurons are highly interconnected with the local pyramidal neurons (Fino and Yuste, 2011), and their influence on the activity of pyramidal neurons depends on their respective subtype (Zhang et al., 2014). Common interneuron markers include parvalbumin (PV), vasoactive intestinal peptide (VIP), somatostatin (SOM), calretinin (CR) and neuropeptide Y (NPY) (Markram et al., 2004). The majority of cortical interneurons express either PV, VIP or SOM, and often co-express CR and/or NPY (Cauli et al., 2014; Gonchar et al., 2008; Markram et al., 2004; Wood et al., 2017; Xu et al., 2010). VIP expressing interneurons receive excitation from inter and intra-areal projections (Harris and Shepherd, 2015). They directly inhibit only a small portion of pyramidal neurons, and mediate disinhibition by targeting predominantly SOM interneurons (Knoblich et al., 2019; Pfeffer et al., 2013). Local excitatory neurons provide input to SOM and PV cells (Harris and Shepherd, 2015), whereas PV cells receive additional feedforward and feedback input from other areas (Yang et al., 2013). SOM interneurons inhibit PV cells in a unidirectional manner, and both of these populations connect to pyramidal neurons, mediating feedback inhibition (Harris and Shepherd, 2015; Pfeffer et al., 2013).

Cortical long-range inputs are thought to modulate sensory processing of the targeted area (Gilbert and Sigman, 2007) and are characterized by specific canonical patterns. L4 is the main recipient of feedforward projections that mostly originate in supragranular layers, while feedback projections

terminate outside of L4 and predominantly emerge from deeper layers (D'Souza and Burkhalter, 2017; Douglas and Martin, 2004; Harris et al., 2019). Thus, the proportion of supragranular long-range inputs is often used as an indicator of the hierarchical order between areas (Barone et al., 2000; Bastos et al., 2015; Douglas and Martin, 2004; Markov and Kennedy, 2013; Markov et al., 2014a). Moreover, the proportion of neurons that contribute to cortico-cortical connections decreases with cortical distance between the two areas (Barone et al., 2000; Douglas and Martin, 2004; Ercsey-Ravasz et al., 2013; Finlay, 2016; Markov et al., 2013; Wang and Kennedy, 2016).

One of the tools to quantify the input to a genetically identified cell type is viral tracing using a genetically modified rabies virus (Wickersham et al., 2007a). The viral glycoprotein gene is deleted, and the virus is pseudotyped with an envelope protein of the avian sarcoma and leukosis virus (EnvA). This limits the primary infection of the virus to cells expressing the avian tumor virus receptor A (TVA), and the virus can only spread from neurons that express the rabies glycoprotein. In this way one can target both the primary infection and the spread to a specific subset of neurons by selectively expressing the TVA receptor and the rabies glycoprotein. However, rabies virus tracing has several caveats. (1) Although there is a considerable amount of data demonstrating that the spread of rabies is biased to synaptically connected neurons (Rossi et al., 2019; Wertz et al., 2015; Wickersham et al., 2007b), it is still unclear how strong that bias is. (2) Rabies virus has been reported to spread anterogradely in primary sensory neurons (Zampieri et al., 2014). (3) Rabies tracing labels at most a small fraction of input cells (Callaway and Luo, 2015). (4) The Cre-lox system used to express the G protein and the TVA receptor is likely not completely tight and will express in Cre-negative cells (Fischer et al., 2019). (5) The rabies virus is cytotoxic (Reardon et al., 2016; Ruigrok et al., 2016; Wickersham et al., 2007b).

To quantify the brain-wide input to the mouse primary visual cortex (V1), we used modified rabies virus to map inter-areal and intra-areal horizontal connections to genetically defined cell types. Using mouse lines that express Cre recombinase in subsets of excitatory neurons in specific cortical layers or interneuron subtypes, we traced monosynaptic inputs to neurons in L2/3, L4, L5, and L6 excitatory neurons, as well as interneurons expressing parvalbumin (PV), vasoactive intestinal peptide (VIP), somatostatin (SST), calretinin (CR) and neuropeptide Y (NPY).

Focusing the analysis on the differences in the distribution of labelled neurons when tracing from different starter neuron populations should reduce the caveat of potential non-synaptic spread. We demonstrated that the area distribution of the presynaptic neurons is similar across neuron subclasses

in V1, which is in accordance with previously described overlapping input patterns in different neuron subclasses of medial prefrontal cortex (Ährlund-Richter et al., 2019). Remarkably, we noted similarities between the V1 and thalamic target distributions, as well as distance-associated decrease in ratio of inputs from L2/3 versus L5.

Results

To identify brain-wide inputs to mouse V1, we used conditional monosynaptic rabies tracing (Wickersham et al., 2007a, 2007b). Using this technology, the primary rabies infection can be targeted to a population of genetically identified starter neurons from which the virus spreads into putative presynaptic neurons. To enable this, the rabies virus is pseudotyped with envelope protein of avian sarcoma and leukosis virus (EnvA) rendering mammalian cells, which do not express the avian tumor virus receptor A (TVA), immune to the infection. In addition, the viral glycoprotein gene essential for transsynaptic spread is replaced with a gene coding for the enhanced green fluorescent protein (EGFP). Both glycoprotein and TVA receptor genes can then be targeted to a genetically identified population of cells using a combination of Cre-driver mouse-lines, and an adeno-associated virus (AAV) to express floxed versions of the glycoprotein and the TVA receptor. This restricts the infection and spread to the genetically targeted subpopulation. We used mouse lines expressing Cre in parvalbumin (PV), vasoactive intestinal peptide (VIP), somatostatin (SST), neuropeptide Y (NPY) or calretinin (CR) expressing interneurons (Gong et al., 2007; Hippenmeyer et al., 2005; Taniguchi et al., 2011) as well as excitatory neurons predominantly in layer 2/3 (Wfs1), layer 4 (Scnn1a), layer 5 (Rbp4), or layer 6 (Ntsr1) (Gerfen et al., 2013; Madisen et al., 2010). We injected AAV2/1-Ef1a-TVA950-T2A-CVS11G into V1 to induce expression of the avian-specific retroviral receptor (TVA) and rabies glycoprotein (CVS11G) (**Figure 2.1A, B**). Retrograde rabies tracing was initiated two days later through injection of an EnvA-coated SADΔG rabies virus in the same location. Mice were sacrificed 5-6 days after rabies injection and brains were removed and prepared for histological analysis. Brains were sliced coronally into 80 µm sections and stained for rabies derived GFP, peptide linker 2A expressed by the AAV, and a neuron-specific nuclear protein NeuN. Starter neurons were identified by the co-expression of the linker peptide 2A from the AAV vector and the GFP from the rabies vector (**Figure 2.1C**). Putative presynaptic cells were identified as 2A negative and GFP positive. Cells were counted manually and mapped to brain regions defined by a mouse reference atlas (Franklin and Paxinos, 2012).

A dense population of starter neurons was found in the V1 with starter neurons restricted to either specific cortical layer or interneuron subtype depending on the mouse line used (**Figure 2.1C**).

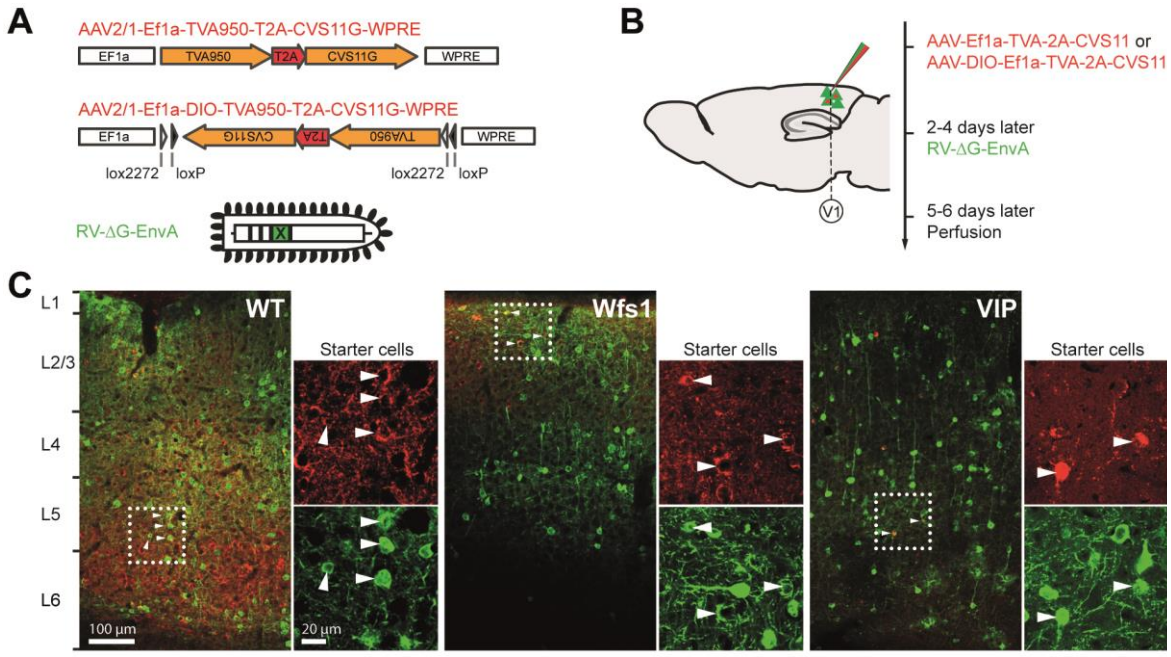

Figure 2.1. Identification of cell-type specific inputs to V1 using retrograde rabies tracing.

(A) Three viral vectors used for monosynaptic rabies tracing: an AAV2/1 that expresses an avian-specific retroviral receptor (TVA) and rabies glycoprotein of the CVS11 rabies strain (CVS11G) either unconditional (top) or conditional (middle), and an EnvA-coated SADΔG rabies virus (bottom).

(B) Experimental timeline. AAV2/1-Ef1a-TVA950-T2A-CVS11G vector was injected in the V1 for unconditional rabies tracing in wild type mice. To target rabies tracing to a genetically defined set of starter neurons, an AAV2/1-Ef1a-DIO-TVA950-T2A-CVS11G vector was injected in V1 of different Cre mouse lines. After 2 to 4 days, the rabies virus was injected in the same location. Animals were sacrificed and perfused five to six days following the rabies injection.

(C) Confocal images of V1 showing starter neurons and rabies labeled cells in different mouse lines. Cells infected by the AAV were identified by staining against the 2A linker peptide (red) and cells infected by the rabies virus by their expression of a GFP variant (green). Cells that were co-infected by both viruses are putative starter neurons. They appear yellow in the merged image and are marked by white arrowheads. WT: wild type (C57BL/6), Wfs1: wolframin ER transmembrane glycoprotein Cre mouse (expresses Cre mainly in layer 2/3 excitatory neurons), VIP: vasoactive intestinal peptide (VIP) Cre mouse (expresses Cre in VIP positive interneurons). The white dotted box indicates the location of the detailed view.

Corresponding presynaptic neurons were found in numerous cortical and subcortical regions of the brain (**Figure S2.1**). In wild type mice, we found an average of 2,179 ± 877 (mean ± SD) labeled starter neurons per mouse throughout all V1 layers, and 30,437 ± 6,112 presynaptic cells throughout the brain areas (**Figure S2.2**). The number of starter neurons as well as presynaptic neurons was lower for the cell-type specific mouse lines, on average 789 ± 237 starter neurons and 12,519 ± 3,159 presynaptic neurons for the layer specific mouse lines and 331 ± 228 starter neurons and 8,476 ± 4,936 presynaptic neurons for the interneuron subtypes.

To compare the contribution of different brain regions in wild-type mice and across conditional mouse lines, we quantified the fraction of presynaptic cells per region as a ratio between the number of presynaptic cells per region and the total number of presynaptic cells (**Figure 2.2A**). In wild type mice

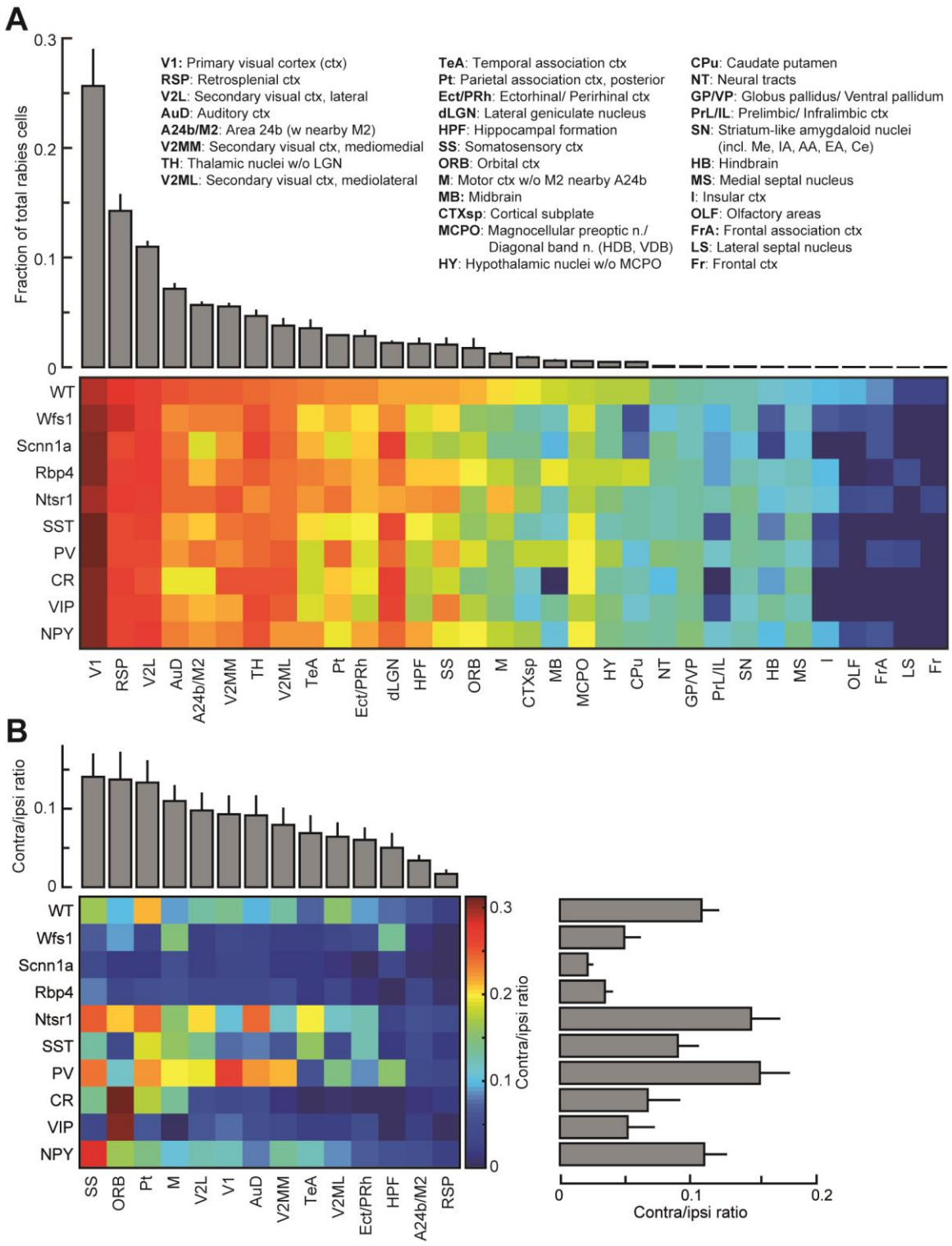

Figure 2.2. Brain-wide distribution of inputs to V1.

(A) Top: Distribution of presynaptic neurons throughout the brain, traced from V1 in three WT mice. Brain regions were identified using a mouse brain atlas (Franklin and Paxinos, 2012). Error bars indicate SEM. Bottom: Fraction of presynaptic cells per region for different mouse lines in which the starter neuron population was restricted to genetically defined excitatory neurons predominantly found in layer 2/3 (Wfs1), layer 4 (Scnn1a), layer 5 (Rbp4), or layer 6 (Ntsr1), or inhibitory parvalbumin (PV), vasoactive intestinal peptide (VIP), somatostatin (SST), neuropeptide Y (NPY), of

calretinin (CR) expressing interneurons. Top row (WT) are the same data shown in the bar plot above. Distribution over areas in all conditional mouse lines is sorted by fraction of the presynaptic cells labeled in wild type mice.
(B) Top: Bar plot indicating ratio of the number of cells in contralateral hemisphere and number of cells in ipsilateral hemisphere in postsynaptic brain areas. Error bars indicate SEM. Bottom left: Ratio of the number of cells in the contralateral hemisphere and number of cells in the ipsilateral hemisphere as a function of starter neuron population and brain areas. Most presynaptic neurons were located in the ipsilateral hemisphere, with strongest callosal inputs in VIP (contra/ipsi: 0.3033) and CR (0.3126) interneurons within orbitofrontal cortex. Bottom right: Ratio of the number of cells in contralateral hemisphere and number of cells in ipsilateral hemisphere from the starter neuron population. Areas of the brain stem and neural tracts were excluded. Strongest callosal inputs were found in layer 6 (Ntsr1, 0.1479) and PV (0.1547) interneurons across all brain areas.

areas with the greatest fraction of presynaptic neurons were V1 (25.65% ± 3.39%, mean ± SEM), secondary visual areas (20.31% ± 1.26%), retrosplenial cortex (14.26% ± 1.56%), auditory cortex (7.15% ± 0.54%) and thalamus (6.89% ± 0.74%). Importantly, area distribution of inputs showed similar patterns across all mouse lines. The presynaptic cells within all mouse lines were mainly found ipsilaterally with respect to the starter neuron population (92.65 ± 3.84%, mean ± SD). Differences in hemispheric origin of input were calculated through the ratio of contralateral versus ipsilateral input. The strongest contralateral input was measured in PV (0.1547, contra/ipsi ratio) and Ntsr1 positive neurons (0.1479) over all brain areas, and for orbitofrontal cortex in CR-Cre (0.3126) and VIP-Cre (0.3033) mouse lines (**Figure 2.2B**).

Next, we wanted to determine the input structures and the distribution of the input from intra-areal, cortical, and subcortical regions to the V1. First, we looked into the connectivity patterns of presynaptic neurons among brain areas with different subclasses of V1 neurons, named divergence patterns. The sum of the neurons in all used conditional mouse lines should allow us to target all neurons labeled in wild type mice. Data from NPY-Cre mice as well as CR-Cre mice was excluded from the analysis due to its overlap with interneuron subtypes of other conditional mouse lines. We quantified the amount of divergence for each source area as a ratio between the sum of neurons from all conditional mouse lines and the number of neurons in wild-type mice normalized by the number of mouse lines. A divergence index of 1 indicates that a cell in the source area contacts all cell types in the V1 with equal likelihood; whereas divergence index of 0 indicates that a cell in the source area converges to one cell type. In general, cortical regions tend to provide more convergent input, while subcortical regions tend to provide more divergent inputs, with lateral geniculate nucleus (dLGN) and V1 providing the largest divergent inputs to V1 (0.6681 and 0.4191, respectively) (**Figure 2.3A**). Overall fraction of the cortical input was larger than the subcortical input regardless of the targeted neuronal subpopulation (86.4 ± 4.7%, mean ± SD) (**Figure 2.3B**), with the bias least pronounced in Scnn1a-Cre (3.22 ± 0.57, cortical/subcortical ratio ± SEM), VIP-Cre (3.00 ± 0.43) and CR-Cre (2.87 ± 0.70)

conditional mouse lines (**Figure 2.3C**). Next, we quantified the similarity of input patterns of different mouse lines between brain areas. We have shown that V1 and its feedforward input regions, especially thalamus, show strongest clustering and are distinct from all other (mainly feedback) input regions to V1 (**Figure 2.3D**).

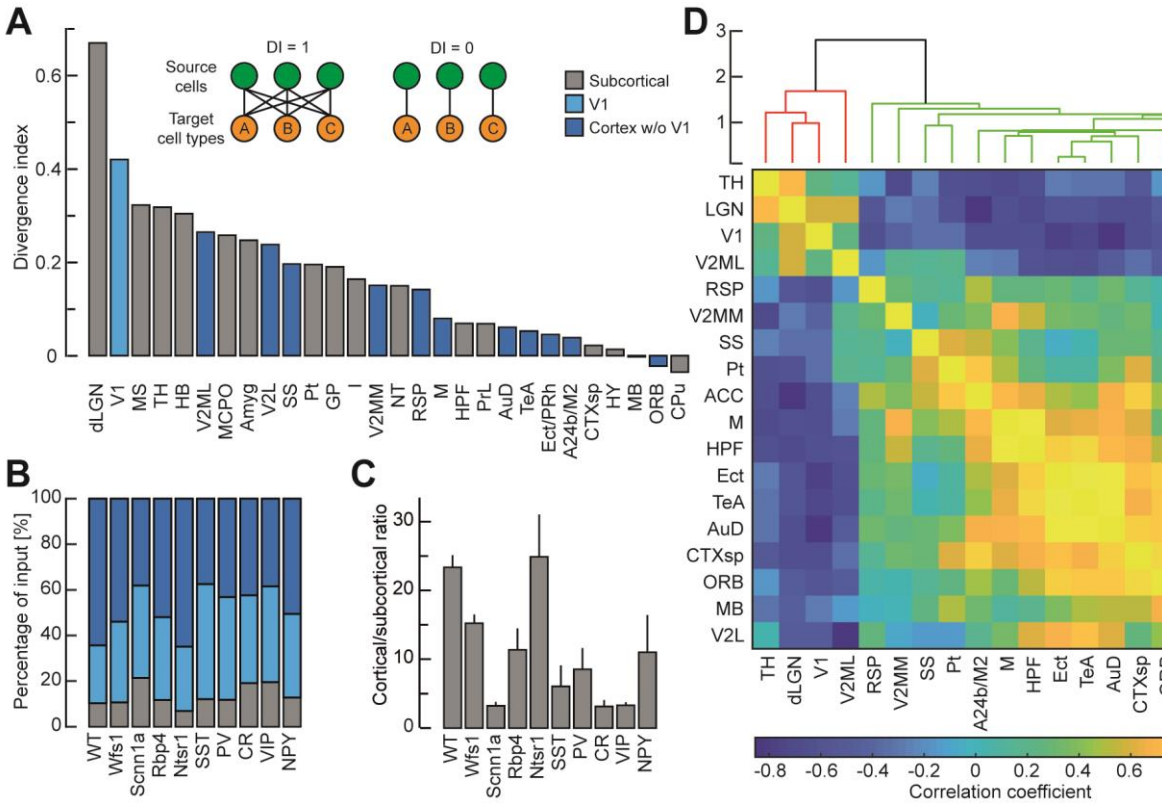

Figure 2.3. Gradual shift in input structure from thalamic, cortical visual, to cortical long-range.

(A) Divergence index for all input areas to V1 with more than 10 cells per brain area in WT mice. A divergence index of 1 would suggest that a cell in the source area contacts all cell types in the target area with equal likelihood. A divergence index of 0 would indicate that a cell in the source area converges to one cell type in the target area. V1, cortical and subcortical regions are colored in light blue, blue and gray, respectively. Inputs from subcortical areas have a tendency to diverge more than inputs from cortical areas.

(B) Percentage of presynaptic neurons labelled in V1, in cortex, and in subcortical structures. On average, 86 ± 1 % (mean ± SEM) of the neurons that provide input to V1 are cortical. Color coding as in **A**.

(C) Ratio of number of neurons labelled in cortical to subcortical regions that send input to V1. Bias towards cortical inputs is least pronounced in Scnn1a-Cre (cortical/subcortical ratio ± SEM: 3.22 ± 0.57), CR-Cre (3.13 ± 0.93) and VIP-Cre (3.23 ± 0.49) conditional mouse lines.

(D) Confusion matrix of correlation coefficients of presynaptic neurons in brain regions that have the highest fraction of presynaptic inputs (>0.6% in wild type mice). The correlation matrix is sorted by hierarchical clustering. V1 and thalamus display strongest clustering and are distinct from other, mostly feedback, input regions. Area V2ML is clustered with V1 and thalamus, however, it shows similarities with both mostly feedforward and feedback areas.

To evaluate characteristics of the laminar distribution of presynaptic neurons in relation to the distance from the starter neurons in the V1, we examined the laminar distribution of cortical areas with the highest fraction of presynaptic neurons in wild type mice (**Figure 2.4**). Intensity profiles of the

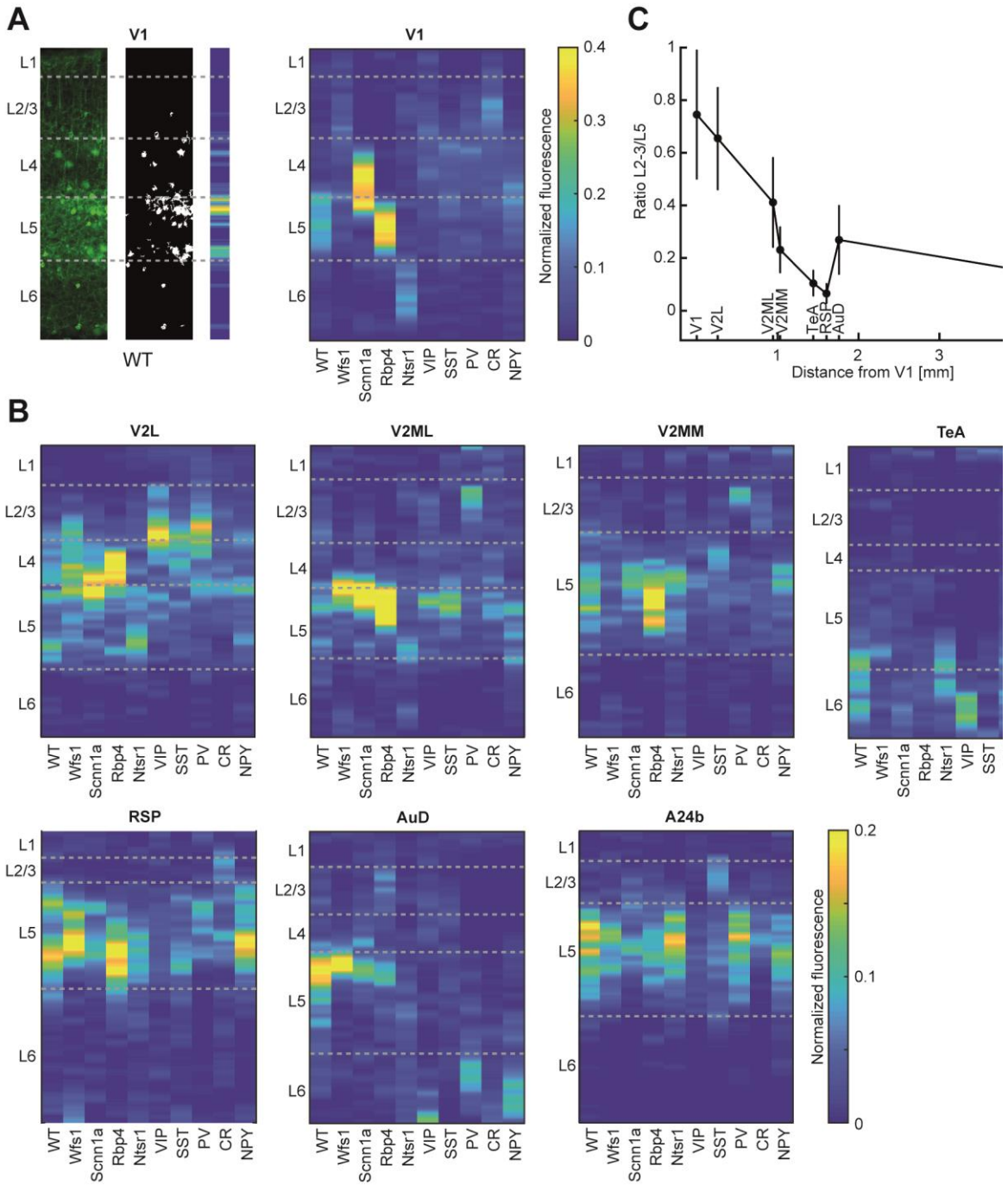

Figure 2.4. Laminar distribution of neurons that provide input to V1.

(A) Left: An example coronal image showing distribution of the rabies positive presynaptic neurons across layers in V1. Boundaries for layers were determined by expression profiles of Cre in different layer specific mouse Cre lines (**Figure S2.3**). To measure laminar density distribution, rabies positive neurons were detected by thresholding. Right: Cellular density distribution across layers in V1 for wild type and conditional mouse lines.

(B) As in **(A)** but for cortical regions with the highest number of presynaptic inputs. Panels of cortical regions are sorted by their distance to V1. Distances were determined by euclidean distance of the centers of mass extracted from a mouse reference atlas (Franklin and Paxinos, 2012).

(C) Contribution of presynaptic inputs across infragranular and supragranular layers as a function of distance from the V1. On average, the proportion of connections made by neurons in L2/3 versus L5 decreases with distance from V1.

layer specific conditional mouse lines for each cortical area were acquired from the database for transgenic characterization of the Allen Brain Atlas. Heat maps demonstrating density of the presynaptic neurons were generated for eight cortical areas (**Figure 2.4A, B**), with layer boundaries determined as intersections of the normalized intensity profiles (**Figure S2.3**). We have demonstrated that the presynaptic populations of intra-areal V1 connections are widely distributed within layers for interneuron subpopulations, and more segregated into specific layers when targeted V1 neurons are restricted to a layer in conditional mouse lines. Moreover, the proportion of infragranular and supragranular presynaptic neuron populations within inter-areal connections changes with distance from the V1. Accordingly, the ratio of connections made by neurons with cell bodies in infragranular layers increases with distance in the long-range connections (**Figure 2.4C**). Noteworthy, most of the layer 5 neurons of retrosplenial and cingulate cortices make not only monosynaptic connections to layer 5 neurons in V1 (Kim et al., 2015) but also to other layers and interneuron subtypes in V1.

Discussion

We used rabies virus tracing to generate a cell-type specific map of the brain-wide inputs to the V1. We have demonstrated a similarity of input patterns among V1 neuron subclasses, as well as a decrease in the ratio of L2/3 to L5 long-range inputs to V1. Surprisingly, we noted a correlation between the projection patterns of V1 and thalamus towards V1.

Technical considerations

It is often assumed that the spread of rabies virus is transsynaptic. However, there is little evidence to show that the spread is exclusively transsynaptic. Much of the data is consistent with a spread that is biased toward synaptic connections, either based on direct measurement of connectivity between labelled neurons (Wickersham et al., 2007b), or by functional correlations between neurons labelled with rabies tracing (Rossi et al., 2019; Wertz et al., 2015). Moreover, as the number of non-synaptic contacts between axon and dendrites is higher than the one of synaptic contacts (Mishchenko et al., 2010), and there is evidence for extra-synaptic exocytosis in addition to the fact that extracellular virions can be detected in extra-synaptic space (Iwasaki et al., 1975), it is possible that viral spread is not restricted to synaptically connected neurons. Much of the early work on the spread of rabies in the nervous system would also be consistent with a spread to axons in the immediate proximity of the site of exocytosis (Ugolini, 1995). Furthermore, anterograde spread of the rabies virus has been shown in sensory neurons (Zampieri et al., 2014).

Rabies tracing labels only a fraction of inputs to starter cells, depending on the levels of G expression in starter cells, initial number of rabies particles entering the cell, and the temporal window before the cell death (Callaway and Luo, 2015). Reduced efficiency to label input cells is most significant for long-range inputs in which higher number of rabies particles and/or input from multiple starter cells is needed for successful labeling (Callaway and Luo, 2015; Miyamichi et al., 2013). Moreover, production of rabies virus, physiological response and resistance of infected cells varies between cell subpopulations of infected cells and for different rabies strains (Reardon et al., 2016; Ruigrok et al., 2016). Physiology of infected neurons can also be altered by rabies induced inflammatory response of the surrounding microglia (Ruigrok et al., 2016).

All these caveats would bias our results to more similar distributions of labelled cells when comparing input patterns to different populations of starter neurons. And indeed, the brain-wide input pattern to the different populations of starter neurons was surprisingly similar for all Cre-mice we tested in this study. This demonstrates that one should be very careful when drawing conclusions based on a dataset in which the tracing was done from only one, or very few, genetically identified populations of starter neurons. We have validated monosynaptic inputs by using CRACM (Leinweber et al., 2017), and kept the incubation times for the helper and rabies virus to a minimum to reduce bias due to cytotoxicity. It is important to note that rabies tracing only reveals presence of the synaptic connection, and not functional properties of the synapse or the connection strength (Callaway and Luo, 2015).

Distributions of brain-wide input to different genetically identified starter neurons are highly similar

Feedforward and feedback connections from other brain areas synapse on both major classes of neurons in cortex – pyramidal neurons and interneurons (Yang et al., 2013). Approximately 80% of the cortical neurons are excitatory pyramidal neurons, while the remaining cells are mostly inhibitory interneurons (Greig et al., 2013; Markram et al., 2004). Pyramidal neurons have relatively stereotypical properties (Kim et al., 2015; Zhang et al., 2019), whereas interneurons are highly diverse in their morphology, physiology, connectivity and laminar location (Ascoli et al., 2008; Fino and Yuste, 2011; Gonchar et al., 2008; Greig et al., 2013; Knoblich et al., 2019; Markram et al., 2004; Niell, 2015; Pfeffer et al., 2013). Axonal projection patterns have been used to address differences between the subtypes of neurons for almost three decades (Fairént et al., 1992), and with the advances in connectivity tracing methods, connectivity patterns are now being more frequently described. Nonetheless, results are often confusing and depend on the methodological approach of the study.

For example, calcium imaging study indicates that the connectivity pattern of PV neurons differs from the pattern of the excitatory neurons in the mouse visual cortex (Hofer et al., 2011). However, we find that area distribution of the presynaptic neurons is similar across all neuron subclasses in V1, with no clear distinction between inhibitory and excitatory neurons or for any other subclass. Similarities in input patterns among different cell types have already been described in mouse medial prefrontal cortex (Ährlund-Richter et al., 2019), and might be addressed to the caveats of the rabies tracing method.

Gradual shift from a bottom-up input pattern to a top-down input pattern

Many aspects of processing within the cortex are conserved among mammals, however, the connection density and functional organization of cells differs within species (Van Hooser, 2007; Niell and Stryker, 2008). For example, mouse cortex is characterized by high levels of connectivity, with even higher probability of an area being connected to visual areas (Gămănuţ et al., 2018; Wang et al., 2012). Whereas, the amount of long-range connections in non-human primates is limited due to higher wiring cost for connecting two distant areas limits (Allman, 1999; Herculano-Houzel, 2012; Horvát et al., 2016), which results in a decreased density of the connectome (Markov et al., 2011, 2014a). However, assuming that the proportion of long range inputs diminishes exponentially with projection distance, as reported in both mice and non-human primates (Barone et al., 2000; Ercsey-Ravasz et al., 2013; Finlay, 2016; Horvát et al., 2016; Markov et al., 2014b; Wang and Kennedy, 2016), the method of binarizing the connections to estimate the connection probability can be misleading. Nonetheless, the present study supports the idea of a highly interconnected visual cortex, with the connection density exponentially decreasing with increasing distance from the V1. Our findings are comparable with recent studies in mouse visual, and medial prefrontal cortices (Ährlund-Richter et al., 2019; Gămănuţ et al., 2018): the majority of connections are local, followed by adjacent areas, other cortical areas and thalamus. Very high intrinsic connectivity has also been reported for area 17 in cat cortex (Binzegger et al., 2004, 2007), whereas in non-human primates approximately 85% of cortical connections are local with 70% of connections formed in 1.5 to 2.5 mm radius from a given postsynaptic cell (Markov et al., 2011, 2013).

Although the lateral geniculate nucleus of the thalamus is the main bottom-up input to visual cortex, it is estimated to provide less than 10% of the total input to V1 in different species (da Costa and Martin, 2009; Da Costa and Martin, 2011; Latawiec et al., 2000). Our data demonstrate that thalamus provides ~7% of total inputs to V1, with one third of the afferents originating from lateral geniculate

nucleus. Surprisingly, thalamus and intrinsic connections of V1 displayed similar target distributions, distinct from other, mostly feedback, brain areas. The only exception was area V2ML which exhibited similarities with both clusters.

Generally, cortical areas provided a higher fraction of inputs than subcortical areas regardless of the targeted neuronal subpopulation, but each connection had a tendency to contact fewer neuronal subclasses than subcortical connections. Top-down cortical connections convey a diverse set of motor and contextual inputs that allow sensory integration and modulate processing of the bottom-up inputs in the V1 depending on the behavioral context (Gilbert and Sigman, 2007). For example, sound driven excitation of auditory cortex alters processing in the V1 by activating inhibitory circuits, and thus inhibiting pyramidal cells (Ibrahim et al., 2016; Iurilli et al., 2012), whereas retrosplenial cortex provides contextual information to V1 such as head position (Vélez-Fort et al., 2018) or other spatially selective visual cues (Powell et al., 2020). Visual cortex also receives information about locomotion (Attinger et al., 2017; Fu et al., 2014), spatial location (Fiser et al., 2016; Saleem et al., 2018), attention (Gilbert and Li, 2013; Zhang et al., 2014), and many other.

Multiple studies have provided evidence that continuity of perception and other aspects of binocularity, such as perception of depth, is assured through callosal projections to the V1 (Cerri et al., 2010; Restani et al., 2009; Zhao et al., 2013). These projections can modulate the response to a visual stimulus in the receiving hemisphere through recruitment of excitatory pyramidal neurons (Kawaguchi, 1992; Kumar and Huguenard, 2001, 2003; Vogt and Gorman, 1982) and inhibitory interneurons (Carr and Sesack, 1998; Cissé et al., 2003, 2007; Petreanu et al., 2007), specifically PV positive cells (Karayannis et al., 2007; Rock and Apicella, 2015; Sempere-Ferràndez et al., 2018). Thus, the effect of the contralateral inputs depends on the balance between direct excitation and disynaptic inhibition of the pyramidal cells. In mice, cell bodies of commissural neurons reside in L2/3 and L5 and to a lesser extent in L6 (Fame et al., 2011). Contralaterally projecting axons of L4 cells get eliminated during postnatal development (De León Reyes et al., 2019), resulting in sparse or absent connectivity (Petreanu et al., 2007; Yamawaki et al., 2014). Callosal axons target neurons in L2/3 and L5, and create sparse connections to neurons in L6 (Petreanu et al., 2007; Rock and Apicella, 2015; Sato et al., 2014; Sempere-Ferràndez et al., 2018). Similar connectivity patterns have been observed in rats (Karayannis et al., 2007; Kawaguchi, 1992; Kumar and Huguenard, 2001, 2003; Palmer et al., 2012; Toldi et al., 1989; Vogt and Gorman, 1982). In cats, callosal-projection neurons terminate throughout all layers of the contralateral cortex with the largest density in the L2/3, lesser in L5 and least in L4 (Carrasco et

al., 2013; Cissé et al., 2003, 2007; Payne et al., 1991). In the present study, L4 neurons received the lowest amount of contralateral versus ipsilateral contacts among layer-specific mouse lines. Surprisingly, the highest ratio of contralateral inputs was found in L6. Within interneuron subclasses, PV neurons received the highest proportion of contralateral versus ipsilateral projections. Interestingly, it has been suggested that PV interneurons serve as the main source of contralaterally driven inhibition of pyramidal cells in mouse retrosplenial cortex (Sempere-Ferràndez et al., 2018), whereas in auditory cortex, callosal projections to PV positive cells selectively suppress the activity of corticocortical L5 pyramidal neurons (Rock and Apicella, 2015).

Fraction of inputs from L5 in comparison with L2/3 decreases with distance of the respective area from V1

Cortical hierarchy is based on the idea that feedback connections project from higher areas of hierarchy towards lower, whereas feedforward connections link areas of lower with higher levels of hierarchy. Cortico-cortical feedback pathways predominantly originate in deeper layers, and have lower weights but are more numerous than feedforward connections which mainly emerge in supragranular layers (D'Souza and Burkhalter, 2017; Douglas and Martin, 2004; Harris and Shepherd, 2015; Markov and Kennedy, 2013; Markov et al., 2014b). Differences between laminar termination patterns of feedback and feedforward projections can be used to assess the hierarchical position of two cortical areas (Barone et al., 2000; Bastos et al., 2015; Douglas and Martin, 2004; Harris et al., 2019; Markov et al., 2014a). Hence, high proportion of supragranular long-range inputs indicates that the areas are close in the hierarchy, a feature commonly used to identify sequence of information processing within cortical areas (Barone et al., 2000; D'souza et al., 2020; D'Souza et al., 2016; Hegdé and Felleman, 2007; Markov et al., 2014a).

Determining cortical hierarchy through laminar distribution of the feedforward and feedback projections has, until know, been mainly used to describe cortical hierarchy in non-human primates, as it was indicated that feedback and feedforward connections in the mouse cortex are not layer specific (Berezovskii et al., 2011). Nonetheless, a recent study reaffirmed that laminar specificity of axonal terminations can be used to address hierarchical arrangement of areas within the mouse visual cortex (D'souza et al., 2020). Our results demonstrate that the fraction of projections from L5, in comparison with L2/3, increases with distance from V1, consistent with the work in non-human primates (Barone et al., 2000; Markov et al., 2014a). This might indicate that the areas in the proximity share similar coordinate systems and may exchange information directly through L2/3 neurons,

whereas distant areas compute the transformation of the coordinate system through additional projection from L5. This would be consistent with the predictive processing framework in which L2/3 cells signal deviations between the actual and expected stimuli, whereas internal representation of the visual scene is stored in L5 neurons (Attinger et al., 2017; Fiser et al., 2016; Heindorf et al., 2018; Keller and Mrsic-Flogel, 2018; Keller et al., 2012; Zmarz and Keller, 2016).

Concluding remarks

Rabies virus tracing is commonly used to investigate cortical connectivity, although precise mechanism of the viral spread is not thoroughly described. To minimize limitations of the method, rabies virus tracing studies should encompass multiple genetically identified populations of starter neurons. Using various mouse lines that express Cre in different subclasses of neurons, we have revealed input similarities among cell subclasses in the V1, and gradual change from a bottom-up to a top-down pattern as a function of the source of projection.

Experimental procedures

Animals and surgery. All animal procedures were approved by and carried out in accordance with guidelines of the Veterinary Department of the Canton Basel-Stadt, Switzerland. Experiments were performed on males and females of ten different mouse lines each on a C57BL/6 background: PV-Cre (Pvalb$^{tm1(cre)Arbr}$ (Hippenmeyer et al., 2005), The Jackson Laboratory, RRID: IMSR_JAX: 008069; n = 3), VIP-Cre (Vip$^{tm1(cre)Zjh}$ (Taniguchi et al., 2011), The Jackson Laboratory, RRID: IMSR_JAX: 010908; n = 3), SST-Cre (Sst$^{tm2.1(cre)Zjh}$ (Taniguchi et al., 2011), The Jackson Laboratory, RRID: IMSR_JAX: 018973; n = 4), CR-Cre (CR$^{tm1(cre)Zjh}$ (Taniguchi et al., 2011), The Jackson Laboratory, RRID: IMSR_JAX: 010774; n = 3), NPY-Cre (NPY$^{RH26Gsat/Mmucd}$ (Gong et al., 2007), MMRRC, RRID: MMRRC_034810-UCD; n = 3), Wfs1-Cre mice (Wfs1-Tg3-CreERT2 (Madisen et al., 2010), The Jackson Laboratory, RRID: IMSR_JAX: 009103; n = 3), Scnn1a-Cre (Scnn1a-Tg3-Cre (Madisen et al., 2010), The Jackson Laboratory, RRID: IMSR_JAX: 009613; n = 4), Rbp4-Cre (Rbp4$^{KL100Gsat/Mmucd}$ (Gerfen et al., 2013), MMRC, RRID: MMRRC_031125-UCD; n = 3), Ntsr1-Cre (Ntsr1$^{GN220Gsat/Mmucd}$ (Gerfen et al., 2013), MMRC, RRID: MMRRC_017266-UCD; n = 4) and C57BL/6J (Charles River Laboratories; n = 3). Mice were group-housed in a vivarium (light/dark cycle: 12/12 hours) and were 71 – 370 days old at the beginning of experiments.

Rabies tracing: Mice were anesthetized using a mix of Fentanyl (0.05 mg/kg; Actavis), Medetomidine (0.5 mg/kg; Actavis) and Midazolam (5.0 mg/kg; Dormicum, Roche). Monosynaptic rabies tracing was initiated by either injecting AAV2/1-Ef1a-TVA950-T2A-CVS11G or AAV2/1-Ef1a-DIO-TVA950-T2A-

CVS11G (titer 2-4*10^{11} GC/ml) into V1 of C57BL/6J mice or of mice of different Cre lines, respectively, through a small craniotomy over V1 (centered on 3.0 mm lateral, and 0.0 mm anterior-posterior from lambda). Following the injection, the skull was sealed with cyanoacrylate and the skin was sutured. After 2-4 days the seal was removed and an EnvA-coated, glycoprotein-G deleted GCaMP6s rabies virus (referred to as EnvA-SADΔG-GCaMP6s, titer 1.5*10^{9} TU/ml, FACS titered (Wertz et al., 2015; Wickersham et al., 2010)) was injected at the same location. For Wfs1-Cre mice, Cre expression was induced by intraperitoneal injection of 100 µl tamoxifen (20mg/ml in saline) twice within a 24-48 h interval 4 days after the AAV injection. 5-6 days after injection of the rabies virus, mice were deeply anesthetized and sacrificed for histological staining. Mice were transcardially perfused for 10 min with phosphate buffered saline (PBS), followed by 10 min of perfusion with a solution of 4% paraformaldehyde (PFA) in PBS. Brains were isolated and post-fixed for 24 h in 4% PFA in PBS. The PFA solution was exchanged for 30% sucrose in PBS, in which brains were immersed until they sank. Afterwards, the brains were transferred to an embedding medium (Tissue-Tek), frozen on dry ice and stored at -80°C before they were sectioned into 80 µm coronal sections using a cryostat. Brain sections were placed in well-plates separately and kept free-floating in PBS. Each section was triple immunostained for rabies derived GFP (Abcam 13970), peptide linker 2A expressed by the AAV (Millipore #ABS31) and a neuron-specific nuclear protein NeuN (Millipore MAB377). The conjugated fluorescent labels of secondary antibodies were Alexa Fluor 488 (Jackson Immuno #703-545-155), Alexa Fluor 568 (ThermoFisher #A10042) and Alexa Fluor 647 (ThermoFisher #A31571), respectively. Stained sections were subsequently mounted on microscope slides and imaged using the ZEISS Axio Scan.Z1 slide scanner with 10x magnification or a Zeiss LSM700 confocal microscope.

Analysis: Data is publicly available (http://data.fmi.ch). Fluorescent images were used to manually count the starter neurons and rabies labeled cells throughout the brain. Starter neurons were identified from the colocalization of green and red fluorophores staining for GFP and the peptide linker 2A included in the AAV. Brain areas were defined as in (Franklin and Paxinos, 2012).

All data analysis was performed using custom-written software written in MATLAB (MathWorks). The contra/ipsi ratio (**Figure 2.2B**) was calculated as the ratio between the number of cells in the contralateral hemisphere and the number of cells in the ipsilateral hemisphere to the starter neuron population. Areas of the brain stem and neural tracts were excluded. The divergence index was calculated for each brain area as a ratio between the number of presynaptic cells across all mouse Cre

lines (except NPY-Cre and CR-Cre) and the number of presynaptic cells for wild-type normalized by the number of total mouse lines:

$$DI(area) = \frac{\frac{\sum^{lines} N(area)}{N_{WT}(area)} - 1}{N_{lines} - 1}$$

The NPY-Cre and Cr-Cre mouse lines were not used for this measure due to the overlap of cell population of other interneuron conditional mouse lines. Using this measure results in numbers between 0 and 1.

The cortical/subcortical ratio (**Figure 2.3C**) was calculated as the ratio between the sum of neurons from the cortical areas with largest fraction of inputs (RSP, V2L, AuD, A24b, V2MM, V2ML, TeA) and dLGN.

Pairwise correlations for each brain region of input fractions for all mouse lines were calculated and hierarchically clustered using the Matlab linkage function (**Figure 2.3D**).

The distribution of presynaptic inputs sorted by layers (**Figure 2.4**) was determined as fluorescence density across each brain region in at least two brain slices at the same locations defined by a mouse reference atlas (Franklin and Paxinos, 2012) and equidistantly spanning the brain region. Density profiles were threshold by 2 standard deviations over the mean and were summed up across animals to get an approximate for the cell density. For better comparison between animals, depth variations within regions were accounted for by interpolation of density profile to a normalized standardized depth. Layer boundaries (**Figure 2.4 and S2.3**) were defined from the intensity profiles of layer specific conditional mouse lines (layer 2/3: Cux2-Cre and Wfs1-Cre; layer 4: Rorb-Cre; layer 5: Etv1-Cre and Rbp4-Cre; layer 6: Ntsr1) from data of the ALLEN Brain Atlas (http://connectivity.brain-map.org/transgenic).

Acknowledgements

We thank Botond Roska for kindly providing the rabies vectors, and Hassana Oyibo and Daniela Gerosa-Erni for production of the rabies and AAV vectors, and the members of the Keller lab for discussion and support. This work was supported by the Swiss National Science Foundation, the Novartis Research Foundation and the Human Frontier Science Program.

Author contributions

M.L. and J.M.S. performed the experiments and analyzed the data. M.M. analyzed the data. M.M. and G.B.K. wrote the manuscript, G.B.K. supervised the project.

Supplementary Figures

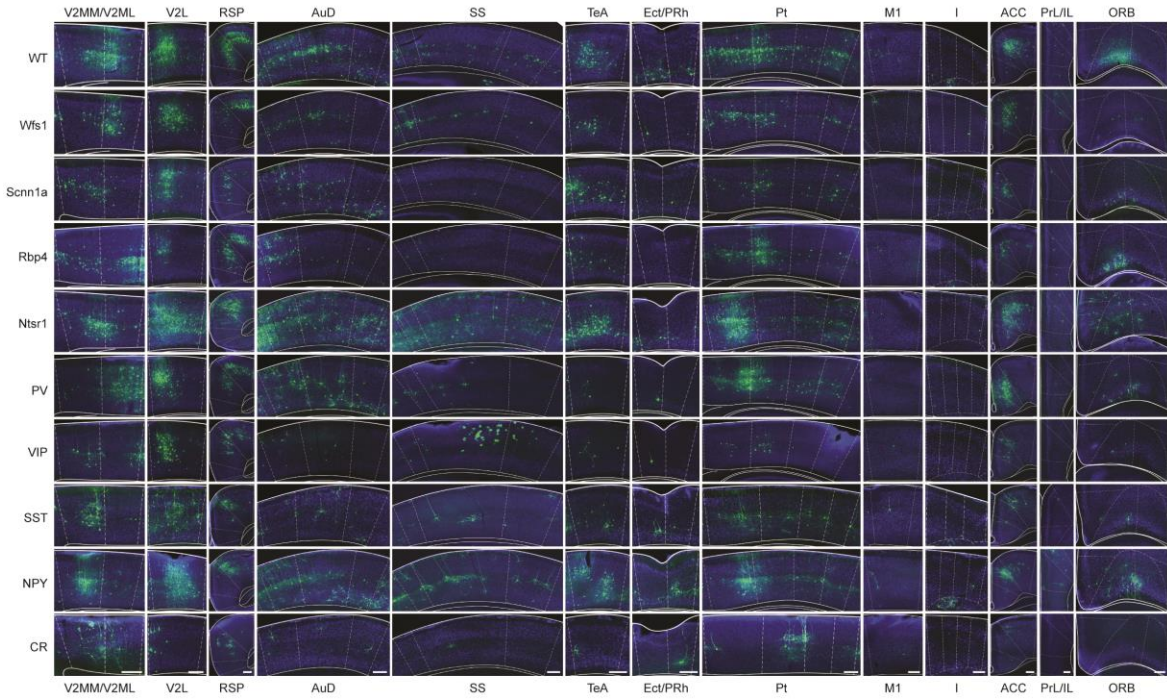

Figure S2.1. Example images of coronal sections of ipsilateral input regions.

Rabies-positive cells are labeled in green. NeuN staining is in blue. PV: parvalbumin positive interneurons, VIP: vasoactive intestinal peptide positive interneurons, SST: somatostatin positive interneurons, NPY: neuropeptide Y positive interneurons, CR: calretinin positive interneurons, Wfs1: expression mainly in layer 2/3, Scnn1a: expression mainly in layer 4, Rbp4: expression mainly in layer 5, Ntsr1: expression mainly in layer 6. Area borders are indicated with white lines.

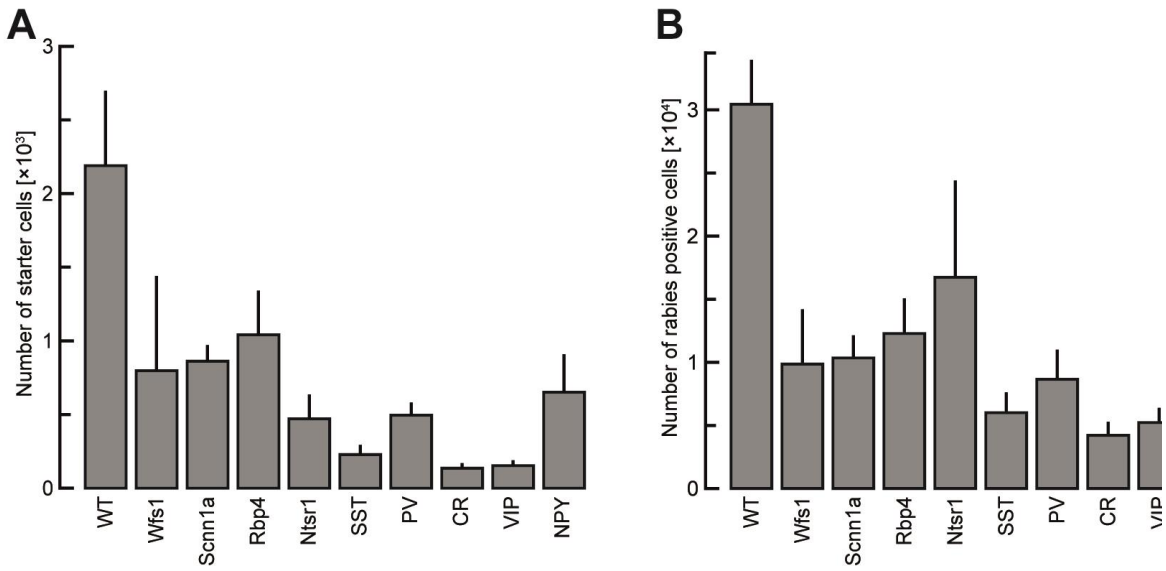

Figure S2.2. Number of starter neurons and rabies positive cells per mouse line.

(A) Average number of starter neurons in V1 for different mouse lines. Here and in the following panel, error bars indicate SEM over mice. Number of starter neurons for cell-type specific mouse lines was lower than in wild type mice (in WT [mean ± SEM] 2,179 ± 507, in layer specific lines 789 ± 118, and interneuron specific lines 331 ± 102).
(B) Average number of presynaptic cells throughout the brain areas for different mouse lines. Number of presynaptic cells for cell-type specific mouse lines was lower than in wild type mice (in WT [mean ± SEM] 30,437 ± 3,529, in layer specific lines 12,519 ± 1,580, and interneuron specific lines 8,476 ± 2,207).

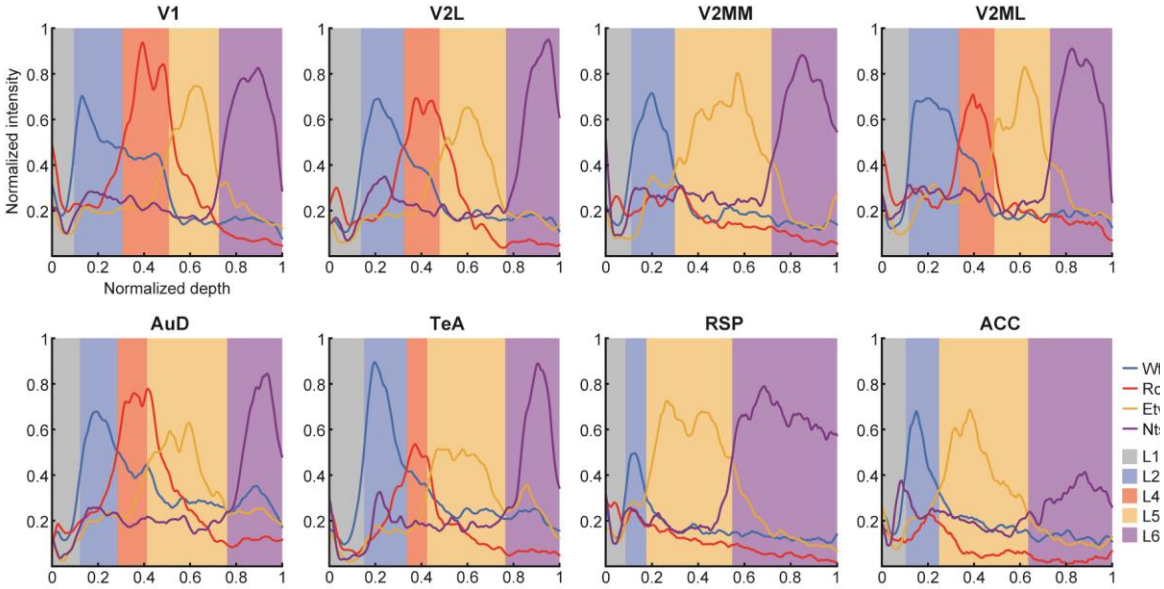

Figure S2.3. Layer identification across cortical regions with the highest number of presynaptic inputs to V1.

Layer boundaries were determined by the intersection of the normalized intensity profiles from layer specific conditional mouse lines. Data was used from the database transgenic characterization of the Allen Brain Atlas. For better estimation of the boundaries, data were pooled for layer 2/3 and layer 5. To account for variation of total depth across the region and between different animals, depth was normalized.

CHAPTER 2: VISUOMOTOR RESPONSES OF THE DORSOMEDIAL STRIATUM

This chapter is based on non-published preliminary data.

In the primary visual cortex (V1), visuomotor learning shapes the long-range connection with A24b/M2 (subregion of the anterior cingulate cortex and adjacent secondary motor cortex). This connection serves as a source of prediction of the input from the retina based on locomotion. Nevertheless, mechanisms in which plasticity between A24b/M2 and V1 is gated is yet to be discovered. It has been hypothesized that deviations between expected stimuli and input from the sensory organs induce plasticity between cortical structures through activation of the basal ganglia circuits. Striatum, the main input structure of circuit, receives projection from layer 5 neurons of mouse V1 (V1-L5) to its dorsomedial part (DMS). Neuronal activity data during visual flow manipulations in a virtual environment demonstrated that both predicted and unpredicted visual stimuli evoke responses in V1-L5 that project to DMS, whereas no clear population responses is elicited in the DMS. Although these results do not support the hypothesis, size of the data set and differences between the experimental procedures make it hard to draw reliable conclusions on the visuomotor processing in the DMS. Efforts should be taken to enlarge the dataset, and address the hypothesis using different experimental approaches.

Introduction

Visuomotor prediction errors, or deviations between the expected (predicted) and actual visual input (from the retina), are thought to be computed in the primary visual cortex (V1) (Attinger et al., 2017; Fiser et al., 2016; Keller et al., 2012; Leinweber et al., 2017; Roth et al., 2016; Zmarz and Keller, 2016). They are established through visuomotor experience (Attinger et al., 2017) and depend on long-range cortical connection with the anterior cingulate cortex and adjacent secondary motor cortex (A24b/M2), whose input serves as a source of prediction in V1 (Fiser et al., 2016; Leinweber et al., 2017). This goes in line with the predictive processing framework of the cortical function (Harris and Mrsic-Flogel, 2013), which hypothesizes that a subset of neurons detects deviations between top-down prediction and bottom-up sensory input. Prediction errors are thought to drive sensorimotor learning (Wolpert et al., 2011), and speculated that they guide the refinement of the internal model in the underlying neural circuitry. Nevertheless, the gating mechanism by which they induce plasticity between motor and sensory areas remains to be discovered.

One of the possibilities is that the prediction error signals are passed through basal ganglia circuits to instruct plasticity between cortical areas involved in sensorimotor learning. Potential of basal ganglia

to gate cortico-cortical plasticity is based on the findings in the songbirds. Zebra finches rely on auditory feedback to learn the vocalization sequence of their tutor (Brainard and Doupe, 2000). Learning is highly dependent on the anterior forebrain pathway, homologue of the basal ganglia circuits in mammals. Prediction errors in vocalizations induce responses in the auditory areas of the avian pallium (Keller and Hahnloser, 2009). These errors are speculated to gate plasticity of the long-range cortical connection between areas responsible for song production through engagement of the anterior forebrain pathway (Luo et al., 2001). Moreover, lesions in any segment of the pathway before the song is learned prevent normal production of the song, but have no effect on the song production once the sequence is learned (Ölveczky et al., 2005).

In rodents, the visual cortex interacts with basal ganglia network through layer 5 projections to the striatum (Khibnik et al., 2014), the main input structure and the largest integrative component of the basal ganglia. Striatal projection neurons, modulated by dopamine, follow direct or indirect output pathways, facilitated by D1 and D2 receptors, respectively. Through interactions between these pathways, dopamine is thought to influence goal-directed behavior by mediating reinforcement or aversion (Gremel and Costa, 2013; Yanike and Ferrera, 2014). Lesion studies in rodents have shown that initial learning driven by the predicted outcome of behavior is conveyed through dorsomedial striatum (DMS). As the behavior is learned, it becomes independent of the reward value, and a dorsolateral part of striatum is needed for its execution (Castañé Anna et al., 2010; Hilario et al., 2012; Mink, 1996; Moussa et al., 2011; Yin, 2010).

Present study consists of preliminary data that were collected with the aim to test the hypothesis that subcortical pathways shape the projection from A24b/M2 to V1 during visuomotor learning in rodents. Primarily, I tried to identify the role of cortical interaction with the striatum in the processing of visuomotor stimuli. The data demonstrate that both neurons in DMS and V1-L5 neurons that project to DMS respond to the onsets of locomotion and reinforcement. Surprisingly, while V1-L5 neurons that project to DMS encode onsets of visual stimuli, neurons in DMS show no clear response to any visual stimuli. Although these results do not support the hypothesis that prediction errors are relayed through the DMS, one should be cautious when interpreting these data because of the size of the dataset and differences between the experimental procedures.

Results

Dorsomedial striatum (DMS) receives strong input from a subregion of the anterior cingulate cortex and adjacent secondary motor cortex (A24b/M2) (**Figure 3.1A**), and primary visual cortex (V1) (**Figure 3.1B**) (Hintiryan et al., 2016). To perform two-photon imaging in dorsomedial striatum, the overlying

cortex was removed, and a cylindrical piece of glass was implanted directly over DMS (**Figure 3.1B, C**). Mice were trained for two days in a coupled visuomotor condition in which flow of the virtual reality was coupled to the locomotion of the mouse (**Figure 3.1D**). Mice were head-fixed on a spherical treadmill surrounded by a toroidal screen that provided full-field visual feedback in the form of gratings on the walls of the virtual corridor (**Figure 3.1D**) (Dombeck et al., 2007; Leinweber et al., 2014). After two training sessions, neural activity in DMS was recorded by two-photon imaging of calcium indicator GCaMP6f (Chen et al., 2013) during different tasks (see Experimental Procedures).

Mismatch task imaging sessions consisted of one or two repetitions of approximately 8 minutes of locomotion coupled to the visual flow feedback (closed loop session), where visual flow was briefly halted for 500 ms at random times (referred to as visual flow perturbations) to probe for the prediction error response. Closed loop session was followed by one session in which the projector was switched off (session in darkness) for 8 minutes. Negative reinforcement in the form of an air puff to the neck was manually introduced to induce running in mice that exhibited low locomotor activity (**Figure 3.1E**). To test visual response, mice were introduced to two repetitions (5.5 min each) of visual response task consisting of presenting randomized oriented drifting gratings (3 s), followed by a gray screen (2 s) (**Figure 3.1F**).

A second group of animals was imaged performing a left-right inverted visuomotor learning task (Leinweber et al., 2017). Mice were water deprived 2 days prior to the experiment to increase their performance in the task. The task required navigating through the grated virtual tunnel towards a water reward region marked by a blue cylinder. In addition, a negative reinforcement (air puff) area was added on the opposite side of the virtual corridor, marked by a green cylinder and walls textured with gray spheres on the black background. Upon arrival to either side, reinforcement was delivered, and 5 s timeout started in which gray screen was shown. Following the timeout, a new trial was initiated by displaying the tunnel in the central position with a spherical wall behind the mouse, and a grated wall in front of the mouse. The width of the tunnel was constant, but length was increased with increased expertise such that mice obtained up to two rewards per minute. The final length of the tunnel was 6 m if the mouse was running in a straight line. Perturbations in the form of the 30° displacement of the visual scenery (tunnel turn perturbations) occurred approximately once per traversal of the tunnel and were restricted to 20% to 80% relative tunnel length but otherwise randomized. Experiments were performed for 8 consecutive days in which 4 such sessions were taken (11 min/session), followed by a session consisting of mice freely behaving in complete darkness. After

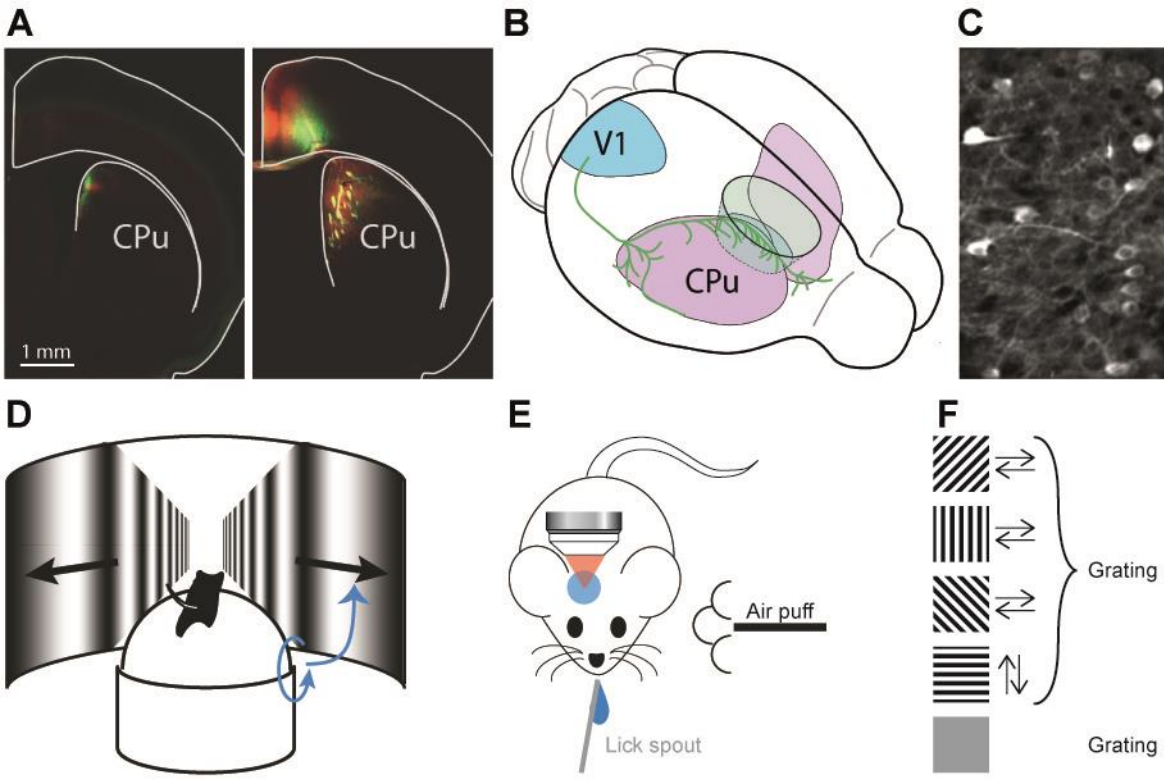

Figure 3.1. Imaging in the dorsomedial striatum (DMS) during behavior – proof of concept and behavioral paradigms used.

(A) Left: Injection of an AAV2/1-Ef1a-eGFP and an AAV2/1-Ef1a-mCherry in V1. Axons are visible in DMS (CPu: caudate putamen). Right: Injection of the same two vectors in A24b/M2. Axons are visible in DMS. Strong yellow signals are axons of passage, and red staining is from terminating axons. Images kindly provided by Dr. Marcus Leinweber.
(B) Schematic of the projection from V1 to DMS and imaging strategy. The cortex over DMS is unilaterally removed to allow for calcium imaging.
(C) Sample two-photon image of DMS neurons labelled by the injection of an AAV2/1-Ef1a-GCaMP6f vector and imaged using the strategy as shown in **(A)**.
(D) Schematic of the setup. Visual flow (black arrows) was coupled to the locomotion of the mouse (blue arrows). In the mismatch and visual response tasks movement was restricted to forward and backward rotation using a pin, whereas in the visuomotor learning task mice could make turns in the environment. Adapted from: (Attinger et al., 2017).
(E) Schematic of the setup with positive and negative reinforcement used in the visuomotor learning task. Adapted from: (Mahringer, 2018).
(F) Oriented grating patterns used in virtual reality for a visual response task.

8 days, mice were given water *ad libitum*. Mismatch and visual response tasks were performed, as previously described, 3 days after the completion of the visuomotor learning task.

To address the activity patterns of the V1 cells that project to DMS, retrograde AAV (Tervo et al., 2016) was injected into the ipsilateral DMS (see Experimental Procedures), and two-photon imaging of calcium indicator GCaMP6f was recorded in the layer 5 neurons of the primary visual cortex (V1-L5). Neuronal activity was recorded in the mismatch, visual response and visuomotor learning tasks (as previously described for the second group of mice). However, there were significant differences in the virtual reality used in the sensorimotor learning task: (1) non-inverted visuomotor learning tunnel was used (Heindorf et al., 2018); (2) there was no negative reinforcement; (3) new trials were initiated by

displaying the tunnel in the same orientation in which mouse finished the traversal, surrounded with sphered walls which were followed by grated walls of the virtual corridor in the direction of the reward. Differences between virtual reality settings eliminated the possibility of performance comparison within experiments, thus performance data were not included in the analysis.

Locomotion changes the activity of neurons in DMS and V1-L5 neurons that project to DMS

Given that both DMS and V1-L5 neurons receive input from the motor cortex, I quantified change in neural processing in these areas during onsets of running and spontaneous turns in the virtual tunnel. As there were no significant differences between running onsets in visuomotor learning and mismatch tasks (data not shown), these data were combined. I found that both DMS (n = 10; 1029 neurons) and V1-L5 neurons that project to DMS (n = 5; 833 cells) increase their overall activity during running onsets (**Figure 3.2A**) in both closed loop session (DMS: 1.91% ± 0.20%; V1-L5: 1.35% ± 0.11%, maximal ΔF/F, mean ± SEM) and darkness (DMS: 1.79% ± 0.18%; V1-L5: 1.28% ± 0.12%). During initiation of ipsiversive (IT) and contraversive (CT) turns, I observed milder increase in the activity in both areas. Whereas onsets of ipsiversive turns in closed loop session had slightly higher peak increase in the population response of DMS neurons (n = 3; 233 cells) than contraversive turns (0.61% ± 0.08%, 0.23% ± 0.06%, respectively), V1-L5 neurons (n = 5,;833 cells) that project to DMS increased their activity independent of the direction of the turn (IT: 0.19% ± 0.05%, CT: 0.20% ± 0.04%) (**Figure 3.2B**). However, when turns were initiated in darkness, increased population response was recorded in both areas independent of the turning direction [IT: 0.50% ± 0.09%, CT: 0.51% ± 0.13% (DMS); IT: 0.40% ± 0.07%, CT: 0.40% ± 0.08% (V1-L5)].

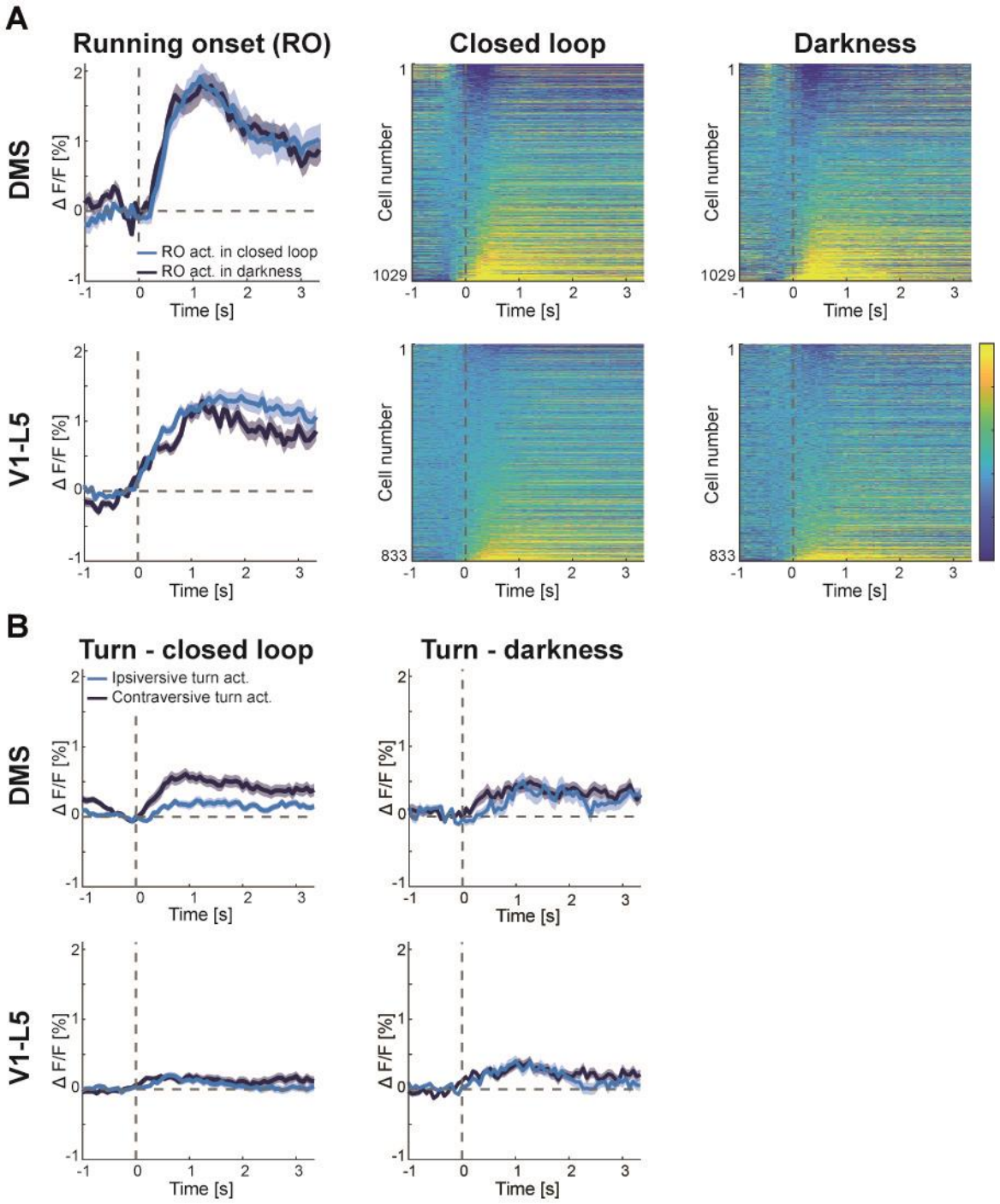

Figure 3.2. Population activity of DMS neurons and V1-L5 neurons that project to DMS changes during locomotion.

(A) Top: Average population response (ΔF/F) to running in closed (light blue) and dark sessions (dark blue) of DMS neurons to running onset (10 animals, 1029 cells) (left), with average responses of individual neurons during closed (middle) and dark sessions (right). Shading indicates SEM. Vertical dashed lines indicate the beginning of the locomotion. Bottom: Same as in the top panel, but for neurons in V1-L5 that project to DMS (5 animals, 833 cells).

(B) Same as in **(A),** left panel but for ipsilateral (light blue) and contralateral turns (dark blue) in closed loop (left) and darkness (right) for DMS neurons (3 animals, 233 cells) (top) and V1-L5 neurons that project to DMS (5 animals, 833 cells) (bottom).

Population of V1-L5 neurons that project to DMS increases activity to visual stimuli and perturbations of the expected visual flow

As running and turn onsets change the visual flow in expected manner, I wanted to inspect whether perturbations of the expected visual flow would alter the activity in DMS or V1-L5 neurons that project to DMS. Both perturbation of the visual flow in the form of a halt or unexpected tunnel turn did not result in a clear population response in DMS neurons (n = 7, 703 cells; n = 3, 233 cells, respectively) (**Figure 3.3A, B**, top panels). On the contrary, visual flow halt (1.44% ± 0.32%, maximal ΔF/F, mean ± SEM), as well as unexpected ipsiversive (1.07% ± 0.21%) and contraversive turns (1.12% ± 0.17%) increased activity in the V1-L5 neurons that project to DMS neurons (**Figure 3.3A, B**, bottom panels) (n = 5, 833 cells). Finally, I tested whether changes in the visual stimuli alter the activity of neurons in

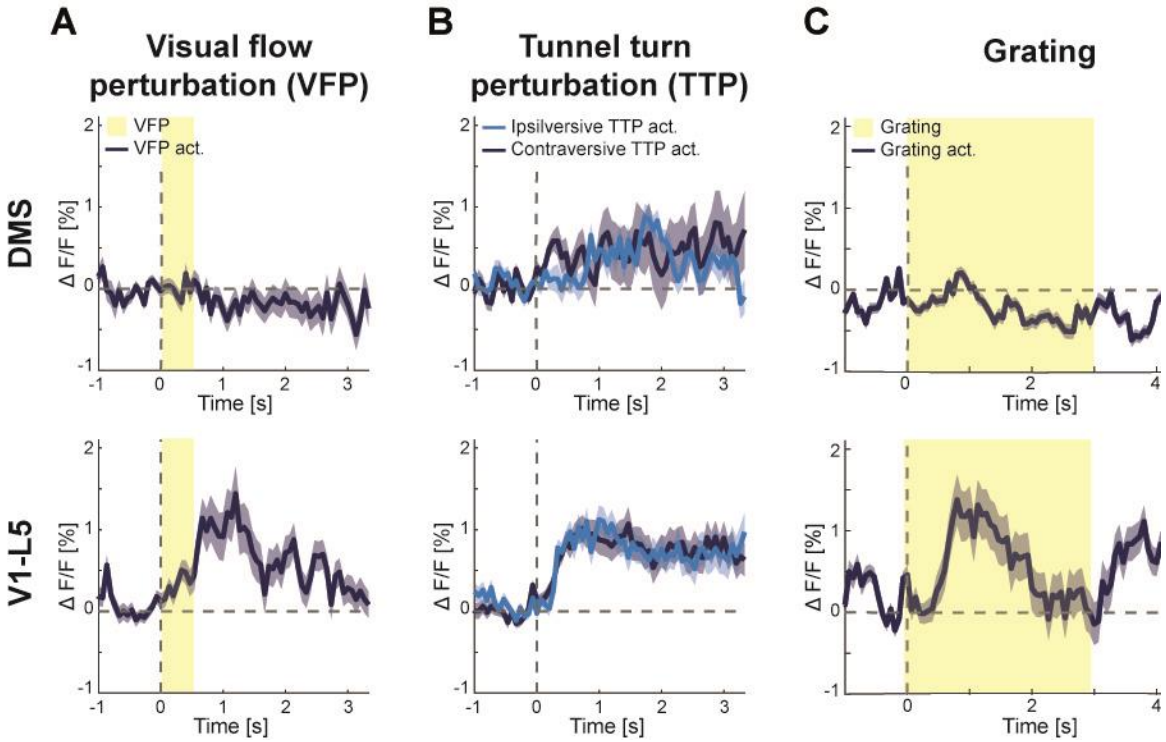

Figure 3.3. Visual stimuli and perturbations of the visual stimuli alter activity patterns in the V1-L5 but not in the DMS.

(A) Average population response (ΔF/F) to perturbation of the visual flow of DMS neurons (7 animals, 703 cells) (top), and V1-L5 neurons that project to DMS (5 animals, 833 cells) (bottom). Shading indicates SEM. Vertical dashed lines indicate the beginning of the stimuli, whereas yellow shading indicates the duration of the feedback perturbation.
(B) Average population response (ΔF/F) to sudden contralateral (light blue) or ipsilateral (dark blue) tunnel turn of 30° of DMS neurons (3 animals, 233 cells) (top), and V1-L5 neurons that project to DMS (5 animals, 833 cells) (bottom). Shading indicates SEM. Vertical dashed lines indicate the beginning of the stimuli.
(C) Average population response (ΔF/F) to perturbation of the visual flow of DMS neurons (5 animals, 471 cells) (top), and V1-L5 neurons that project to DMS (4 animals, 653 cells) (bottom). Shading indicates SEM. Vertical dashed lines indicate the beginning of the stimuli, whereas yellow shading indicates the duration of the grating pattern.

DMS and V1-L5 neurons that project to DMS when the animal is stationary using a visual response task. As animals were accustomed to the virtual reality, onsets of grating in which the animal was

stationary were sparse. Thus, onsets of all 4 different gratings (each shifting in two possible directions) were combined in the analysis. Whereas DMS did not have a clear visual response to grating stimuli (**Figure 3.3C**, top panel), V1-L5 neurons (n = 4, 653 cells) that project to DMS increased their activity during the onset of gratings (1.38% ± 0.31%) as well as presentation of the gray screen (1.11% ± 0.19%) (**Figure 3.3C**, bottom panel).

Reinforcement influences neuronal activity in DMS and V1-L5 neurons projecting to DMS

Lastly, I wanted to address the effects of reinforcement on neuronal population activity in DMS and V1-L5 cells that project to DMS. Neuronal response to positive reinforcement (water reward) changed during the experiment in both brain areas (**Figure 3.4A**). In the last three days of the visuomotor learning task (days 6-8) there was a decrease in the activity in comparison with the first three days of the experiment in both brain areas. However, in V1-L5 cells that project to DMS (n = 4, 708 cells) there is less variability within individual onsets and animals than in DMS neurons (n = 3, 233 cells). On the contrary, negative reinforcement increased neuronal population activity in both brain areas with 2.69% ± 0.82% (mean ± SEM) maximal ΔF/F in DMS (n = 6, 519 cells), and 7.29% ± 1.25% (at 0.933 s) in V1-L5 neurons projecting to DMS (n = 3, 329 cells) (**Figure 3.4B**). Note that negative reinforcement

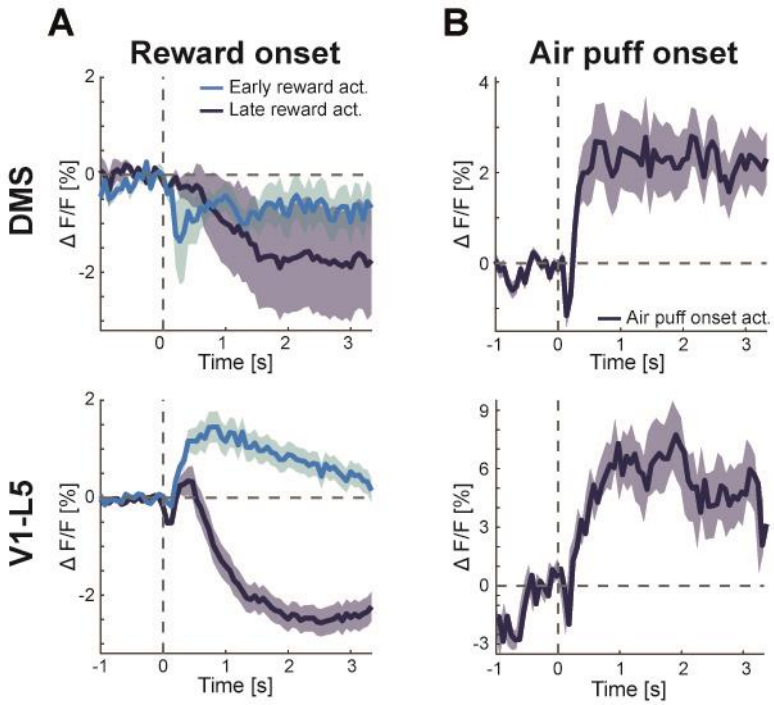

Figure 3.4. Negative and positive reinforcements alter population response of DMS neurons and V1-L5 neurons that project to DMS.

(A) Average population response (ΔF/F) to water reward of DMS neurons (3 animals, 233 cells) (top) and V1-L5 neurons that project to DMS (4 animals, 708 cells) (bottom) during the first 3 days (light blue) and last 3 days of the experiment (dark blue). Shading indicates SEM. Vertical dashed lines indicate the beginning of the stimuli.

(B) Average population response (ΔF/F) to the air puff of DMS neurons (6 animals, 519 cells) (top) and V1-L5 neurons that project to DMS (3 animals, 529 cells) (bottom). Shading indicates SEM. Vertical dashed lines indicate the beginning of the stimuli.

was not used in the visuomotor learning task while imaging V1-L5 neurons that project to DMS, and presented data were acquired in mice during the mismatch task. While recording DMS neurons in the visuomotor learning task, animals learned to avoid negative reinforcement zones early in the trial. As air puffs were no longer used later in the trial, neuronal activity data from mismatch and visuomotor learning tasks were combined.

Discussion

With these experiments I tried to identify the role of cortical interaction with striatum, the main input area of basal ganglia circuits, in processing visuomotor stimuli. I have shown that both neurons in DMS and V1-L5 neurons that project to DMS respond to onsets of locomotion and reinforcement. Surprisingly, although neurons in V1-L5 cells that project to DMS respond to visual stimuli, neurons in DMS show no clear response to these stimuli.

Technical considerations

One of the shortcomings of 2-photon imaging in the DMS is insufficient long-term stability of the surgical preparation in comparison with the surgical procedures for imaging cortical structures. In cortical surgical preparation edges of the implanted window adhere to the skull. However, a window implanted on the surface of the DMS is attached to the skull through a vertical, thin layer of glue, enabling more movement at the imaging site which led to inflammatory response of the surrounding tissue and movement artefacts. Because of that, a large amount of DMS data was incomplete and thus excluded from the dataset. Hence, it would be advisable to use implants which do not allow for movement such as gradient index (GRIN) lenses (Levene et al., 2004) or glass plugs (Velasco and Levene, 2014) when imaging DMS. Unfortunately, efforts to expand the DMS dataset, for reasons that remain unclear, led to insufficient labeling for 2-photon imaging (see Experimental Procedures).

Furthermore, retrograde labeling of V1 neurons that project to DMS has resulted in abundance of labeled neurons across layers 2/3 and 5. However, earlier study has shown that over 80% of V1 neurons that project to DMS are distributed within layer 5 (Khibnik et al., 2014), indicating that the labeling used in this study might be unreliable. I speculate that this might be caused by a malfunctioning injection system that leaked viral particles to overlying motor cortex, cingulum, or the lateral ventricle, thus infecting neuronal cell bodies at the site of exposure and mediating retrograde labeling. However, as the precise mechanisms of retrograde transport remain to be discovered, one could speculate that excessive labeling might be explained through imperfections of the retrograde transport of the AAV.

In addition, size of the dataset and differences between the experimental procedures in the learning paradigm of the two areas of interest make it difficult to make conclusions about the processing of the visuomotor stimuli in the DMS. Hence, one should be cautious when interpreting these results and effort should be taken to repeat these experiments and introduce other experimental procedures.

Subcortical areas and long-range cortical plasticity

When the motor area produces a motor output, it sends efference copy to sensory areas (corollary discharge). Sensory areas use corollary discharge to predict the expected sensory input resulting from the initiated movement. It has been proposed that the source of the prediction of visual input in V1 is a subregion of the anterior cingulate cortex and adjacent secondary motor cortex (A24b/M2) (Fiser et al., 2016; Leinweber et al., 2017). This long-range cortical input is shaped by visuomotor experience, but mechanisms that shape the connection are still unclear. In the songbird, anterior forebrain pathway (AFP, analogous to mammalian basal ganglia) is critical for learning of the long-range connection between HVC and RA (motor areas of avian pallium) which allows sensorimotor learning of the song by a tutor (Andalman and Fee, 2009; Fee and Goldberg, 2011; Ölveczky et al., 2005). AFP circuits drive vocal variability (Kao et al., 2005; Ölveczky et al., 2005; Scharff and Nottebohm, 1991) and evaluate errors which are thought to guide plasticity in the motor pathway (Bottjer et al., 1984; Troyer and Bottjer, 2001).

Based on findings in songbirds, it has been speculated that the visuomotor plasticity in mammals might be gated through subcortical pathways connecting A24b/M2 to V1. Both A24b/M2 and V1 interact with basal ganglia through a projection to striatum, the main input structure and the largest integrative component of the basal ganglia (Hintiryan et al., 2016). If subcortical pathways guide the long-range cortical plasticity, prediction errors would be passed through the basal ganglia to instruct plasticity between A24b/M2 and V1. My research has shown that V1-L5 cells that project to DMS seem to convey information about changes in the visual field, rather than prediction errors alone, with no population response to prediction error in the DMS. Previous studies have found that the corticostriatal axons originating in V1 are functional and evoke responses in the DMS (Khibnik et al., 2014; Reig and Silberberg, 2014; Wang et al., 2018). Surprisingly, in the present study visual stimuli did not alter average population response in the DMS.

Lesion studies in rodents have indicated that striatum is necessary for habit formation (Balleine and Dickinson, 1998; Belin et al., 2009; Yin and Knowlton, 2006; Yin et al., 2004). DMS is needed to consolidate goal-directed behaviors, whereas dorsolateral part of the striatum (DLS) is required for habitual performance after the behavior is learned. In nonhuman primates, areas that correspond to

DMS and DLS (associative and sensorimotor districts of striatum (Graybiel, 2008)) display similar shifts in activity as noted in rodents (Hikosaka et al., 1999; Miyachi et al., 1997, 2002). However, in this study the average population responses of V1-L5 neurons that project to DMS and DMS neurons to visual stimuli and locomotion stayed stable over training sessions (data not shown), whereas their response to reward changed over time. This supports the idea of a critical transition period during habit formation after which the behavior becomes independent of the reward value (Dickinson, 1985).

Future directions

Throughout this research, I have gained insight on the ways DMS computes incoming visual and motor stimuli. However, size of the dataset and differences between the experimental procedures make it difficult to make an evidence-supported conclusion about the processing of the incoming information from V1 to DMS. Thus, the current dataset should be expanded, and different experimental approaches should be considered.

Firstly, to investigate the effect of the DMS on the plasticity of the long-range cortical connection between A24b/M2 and V1, one should describe input to DMS from these areas. This might be done by retrograde labeling of neurons that project to the DMS using retro-AAV virus (Tervo et al., 2016) as done in this study, or with a functionalized non-toxic transsynaptic rabies variant (Chatterjee et al., 2018). Another approach would be recording from the axons in the DMS.

Secondly, using layer and population specific Cre-lines could provide insight on the significance of each neuronal population in processing visuomotor information. For example, it has been shown that the main source of projection to DMS from V1 are layer 5 intratelencephalic neurons (Khibnik et al., 2014). Hence, one could use Tlx3-Cre mouse line (Gerfen et al., 2013) to inspect the responses to visuomotor stimuli in this subpopulation of neurons. It has been demonstrated that striatal neurons expressing D1 or D2 dopamine receptors differ in their functionality (Keeler et al., 2014). Hence recordings in the DMS should be done separately in neurons expressing dopamine receptor D1 and D2, for example by using EY217-Cre and ER43-Cre mouse lines (Gerfen et al., 2013; Gong et al., 2007), respectively.

Finally, optogenetic manipulations would allow the researcher to gain further insight on subcortical processing of the visuomotor stimuli, and possibly reveal mechanisms in which subcortical processing of prediction error signals promotes activation of the local circuit in A24b/M2.

Experimental procedures

Experimental Model and Subject Details

All animal procedures were approved by and carried out in accordance with guidelines of the Veterinary Department of the Canton Basel-Stadt, Switzerland. Data for all the experiments were collected on female C57BL/6J (Charles River Laboratories). Mice were group-housed in a vivarium (light/dark cycle: 12/12 hours).

Experiments started with a surgery, and the data were collected as follows:

1. For Figure 3.2.

Panel A DMS data: n = 10, 1029 cells, P80 – P81; V1-L5 data: n = 5, 833 cells, P127 – P128

Panel B DMS data: n = 3, 233 cells, P80 – P81; V1-L5 data: n = 5, 833 cells, P127 – P128

2. For Figure 3.3.

Panel A DMS data: n = 7, 703 cells, P80 – P81; V1-L5 data: n = 5, 833 cells, P127 – P128

Panel B DMS data: n = 3, 233 cells, P80 – P81; V1-L5 data: n = 5, 833 cells, P127 – P128

Panel C DMS data: n = 5, 471 cells, P80 – P81; V1-L5 data: n = 4, 653 cells, P127 – P128

3. For Figure 3.4.

Panel A DMS data: n = 3, 233 cells, P80 – P81; V1-L5 data: n = 4, 708 cells, P127 – P128

Panel B DMS data: n = 6, 519 cells, P80 – P81; V1-L5 data: n = 3, 529 cells, P127 – P128

Surgical procedures

Anesthesia. Before any surgical procedure, mice received an intraperitoneal injection of a mixture of fentanyl (Fentanyl-Mepha, Mepha, 0.05 mg/kg), midazolam (Dormicum, Sintetica, 5.0 mg/kg), and medetomidine (Dormitor, Pfizer, 0.5 mg/kg). Subcutaneous injection with a mixture of lidocaine (Xylocain, Aspen pharma Schweiz, 10 mg/kg) and ropivacaine (Naropin, AstraZeneca, 3 mg/kg,) was injected in the surgical area to reduce post-operative pain. After the surgery, intraperitoneal injection with a mixture of flumazenil (Anaxete, Roche, 0.5 mg/kg) and atipamezole (Antisedan, Orion Pharma, 2.5 mg/kg) was injected to reverse anesthesia. Buprenorphine (Suboxone, Reckitt Benckiser Healthcare UK Ltd, 0.1 mg/kg) and meloxicam (Metacam, Boehringer Ingelheim, 5 mg/kg) were applied subcutaneously, and meloxicam was injected again for the next two days at an interval of 24 h to assure analgesia overnight.

Surgical procedure for imaging V1. A Circular piece of scalp was removed, and the underlying bone was cleaned and dried. Temporalis muscles were slightly detached, and the skull was scored with a needle and covered with Histoacryl (B. Braun) to increase adhesion with glue and dental cement. A 4 mm craniotomy was made over the right V1, centered on 2.5 mm lateral and 1 mm anterior of lambda.

A 4 mm circular cover glass was glued in place using gel superglue (Ultra Gel, Pattex). Neurons were labeled with a calcium indicator by injecting retrograde AAV Ef1a-GCaMP6f (titer $1.7*10^{11}$ GC/mL) into the ipsilateral DMS. Two injections were distributed 2.1 mm deep through small craniotomies centered on 0.3 and 0.8 mm anterior, and 2 mm lateral of bregma (approx. 100-150 nL per injection), and the craniotomies were then sealed with gel superglue. A titanium head bar was fixed to the skull using dental cement (Paladur, Heraeus Kulzer) (Leinweber et al., 2017). V1 was mapped with intrinsic signal imaging, as previously described (Wertz et al., 2015).

Surgical procedure for imaging DMS. A Circular piece of scalp was removed, and the underlying bone was cleaned and dried. *Temporalis* muscles were slightly detached, and the skull was scored with a needle and covered with Histoacryl (B. Braun) to increase adhesion with glue and dental cement. A 3.5 mm craniotomy was made over the right DMS, centered on 2.0 mm lateral and 0.3 mm anterior of bregma. The dura was removed, and the overlying cortical tissue was carefully aspirated by a blunted 21-gauge needle (Sterican, B. Braun) to the surface of the corpus callosum fibers. The *superior sagittal sinus* was avoided and remained unaffected by aspiration in all experiments. To reduce effects of blood coagulation on imaging quality, bleeding from larger vessels was treated with sterile absorption spears (Sugi Absorption Triangles, Agnthos) and cleaned with the PFA. Neurons were labeled with a calcium indicator by injecting AAV Ef1a-GCaMP6f (titer $1.4\text{-}2.2*10^{11}$ GC/mL) into the right monocular DMS, centered on 1 mm lateral and 0.8 mm anterior of bregma (5-7 injections per mouse, approx. 50-100 nL per injection). A 3 mm circular cover glass was placed on top of the tissue, and carefully pressed with a glass pipette into the tissue (0.1 – 0.2 mm) to reduce effects of the injury-induced brain swelling on imaging quality. Window was glued in place by carefully applying gel superglue (Ultra Gel, Pattex) with bent 31-gauge needle (BD-Veo, BD) on the exposed surface of the cortical tissue, overlying skull, and corners of the window (**Figure 3.1A**). Manually modified titanium head bar was fixed to the skull using dental cement (Paladur, Heraeus Kulzer) (Leinweber et al., 2014).

I attempted to do additional experiments to expand the dataset and include additional experimental procedures. However, for reasons that are still unclear, further experiments led to very low labeling which was insufficient for 2-photon imaging. Use of a different titer or strain of the virus, increasing the injection volume, adjusting craniotomy and injection location, modulating surgical procedure and post-surgical window cleaning did not resolve this problem. Kwik-Sil or similar products were not used as the learning task requires chronic imaging, and it was demonstrated to be a favorable substrate for bacterial growth in previous work of the lab personnel. As the expression was visible under the fluorescence microscope, it could be speculated that the reason for the lack of expression under the 2-photon microscope may be lateral or medial movement of the dorsal striatum in the right ventricle,

making the initial injection location inaccessible. However, because of the vast amount of resources used to address the above-mentioned issue with no success, the project was discontinued.

Virtual reality and behavior

Experimental setup. All calcium imaging experiments were performed on a custom-built two-photon microscope setup as previously described (Leinweber et al., 2014). During all experiments, running speed and direction of the mouse, visual flow speed, reinforcement onsets, as well as pupil position and diameter were recorded.

Mismatch task (prediction error paradigm). Each experiment consisted of 2-5 imaging days with 2 imaging sessions (8 min/session) with different virtual reality modules. Rotation of the spherical treadmill was restricted to forward and backward rotation using a pin. In the closed loop session, movement of the virtual tunnel was coupled to the locomotion of the mouse, and perturbations (mismatch events) were randomly generated by halting the visual field for 0.5 s. Following open loop sessions, mice were imaged in complete darkness. To initiate movement, negative reinforcement (mild air-puff) was manually introduced. Air-puff initiated movement onsets were excluded from movement onset calculations.

Visual response task. Following the mismatch task experiment, mice were introduced to the virtual reality to test visual response (5.5 min/session). Two of these sessions were done per day, separated by an average of 24 hours. Oriented grating patterns were presented for 3 seconds in a randomized manner, separated by 2 seconds timeout (gray screen).

Visuomotor learning task. Mice were water restricted for the duration of the experimental series and were supplemented with water if they received less than 1 mL of total water reward. The weight of all mice was monitored daily to ensure that body weight does not drop below 80% of the starting weight. Water was provided *ad libitum* after the last training session.

Mice were initially placed into a virtual environment with an infinite tunnel (as described in the mismatch task, but with no perturbations) in two separated training sessions to allow the mice to get accustomed to the setup. Rotation of the spherical treadmill was restricted to forward and backward rotation using a pin. During the experiments, the rotation of the ball was no longer restricted, and mice could make turns in the virtual environment. Visuomotor data was gathered through 8 consecutive days. Each day 4 visuomotor learning task sessions and one session in darkness were performed (total of 52 min per day per animal).

The virtual reality for imaging V1 consisted of a tunnel with a positive reinforcement zone located at one end of the tunnel. The walls of the tunnel were textured with white circles on a black background in the first half of the tunnel and sinusoidal vertical stripes in the second half. Reaching the positive reinforcement zone triggered a 5 s timeout during which the mouse could lick from a waterspout to collect the reward. After the timeout, the virtual environment was reset to the beginning of the tunnel on the X-axis, whereas the location on the Y-axis and angle changed depending on the parameters during reward collection. As the mouse's performance in the task improved, the length of the tunnel with sinusoidal vertical stripes was gradually increased to keep the rewards per hour at an approximately constant level of 100, throughout training. Three days after the visuomotor learning task, mice were subjected to one session of the mismatch and visual response tasks.

Reaching the positive reinforcement zone in the virtual reality used for imaging DMS triggered previously described timeout. However, the virtual reality was reset to the border of the two textures of the tunnel (on the X-axis), middle of the tunnel on the Y-axis, and with the angle facing the reward zone. In addition, a negative reinforcement zone (10 ms air puff) was introduced at the opposite end of the tunnel, and it did not affect the mouse position. Positive and negative reinforcements were distinguished by both color and pattern of the virtual walls. Positive reinforcement was at the end of the striped tunnel and presented as a blue cone positioned at the upper part of the tunnel. Negative reinforcement was at the end of the wall with white circles and presented as a green cone positioned on the bottom of the tunnel. Moreover, positions of the left and right were reversed; during a left turn, the virtual reality would turn to the right and vice versa. Two days after the end of the experiment ended, mice were tested in the mismatch and visual response tasks on 3 consecutive days.

Quantification and Statistical Analysis

Extraction of neuronal activity. Calcium imaging data were processed as previously described (Keller et al., 2012) and all data analysis was done in MATLAB (MathWorks). Raw images were registered to correct for brain motion, and neurons were manually selected based on mean and maximum fluorescence images. ΔF/F traces were calculated as mean fluorescence in a selected region of every imaging frame and subsequently subtracted and normalized by the median fluorescence.

Data analysis. To quantify average response traces, event-triggered fluorescence trace for each neuron was calculated as an average response between events in the session. Responses of all neurons were averaged and the baseline (mean ΔF/F in a 0.3 s window pre-event onset) was subtracted. Specific conditions were set for events to be included in the analysis.

1. For perturbations and turns mice had to be running above threshold (10^{-2} cm/s) for at least 1 s before and after event onset.
2. For running onset mice had to be stationary 1 s before and move above threshold 1 s after the event onset. Air-puff induced running onsets were excluded from the analysis.
3. For grating onsets, mice had to be stationary 1 s before and 1 s after the onset of the event.

Furthermore, data from animals with less than 3 event onsets were not included in the analysis. Because of the small size of the data set, additional analysis and further splitting of the dataset was avoided. In addition, differences in the virtual reality for visuomotor learning used for DMS and V1-L5 dataset eliminated the possibility of performance comparison within these experiments. Thus, these data were not included.

REFERENCES

Ährlund-Richter, S., Xuan, Y., van Lunteren, J.A., Kim, H., Ortiz, C., Pollak Dorocic, I., Meletis, K., and Carlén, M. (2019). A whole-brain atlas of monosynaptic input targeting four different cell types in the medial prefrontal cortex of the mouse. Nat. Neurosci. *22*, 657–668.

Allman, J.M. (1999). Evolving brains.

Andalman, A.S., and Fee, M.S. (2009). A basal ganglia-forebrain circuit in the songbird biases motor output to avoid vocal errors. Proc. Natl. Acad. Sci. U. S. A. *106*, 12518–12523.

Ascoli, G.A., Alonso-Nanclares, L., Anderson, S.A., Barrionuevo, G., Benavides-Piccione, R., Burkhalter, A., Buzsáki, G., Cauli, B., DeFelipe, J., Fairén, A., et al. (2008). Petilla terminology: Nomenclature of features of GABAergic interneurons of the cerebral cortex. Nat. Rev. Neurosci. *9*, 557–568.

Attinger, A., Wang, B., and Keller, G.B. (2017). Visuomotor Coupling Shapes the Functional Development of Mouse Visual Cortex. Cell *169*, 1291-1302.e14.

Baker, A., Kalmbach, B., Morishima, M., Kim, J., Juavinett, A., Li, N., and Dembrow, N. (2018). Specialized subpopulations of deep-layer pyramidal neurons in the neocortex: Bridging cellular properties to functional consequences. J. Neurosci. *38*, 5441–5455.

Balleine, B.W., and Dickinson, A. (1998). Goal-directed instrumental action: Contingency and incentive learning and their cortical substrates. In Neuropharmacology, (Pergamon), pp. 407–419.

Bar-Gad, I., Morris, G., and Bergman, H. (2003). Information processing, dimensionality reduction and reinforcement learning in the basal ganglia. Prog. Neurobiol. *71*, 439–473.

Barone, P., Batardiere, A., Knoblauch, K., and Kennedy, H. (2000). Laminar distribution of neurons in extrastriate areas projecting to visual areas V1 and V4 correlates with the hiearchical rank and intimates the operation of a distance rule. J. Neurosci. *20*, 3263–3281.

Bastos, A.M., Vezoli, J., Bosman, C.A., Schoffelen, J.M., Oostenveld, R., Dowdall, J.R., DeWeerd, P., Kennedy, H., and Fries, P. (2015). Visual areas exert feedforward and feedback influences through distinct frequency channels. Neuron *85*, 390–401.

Belin, D., Jonkman, S., Dickinson, A., Robbins, T.W., and Everitt, B.J. (2009). Parallel and interactive learning processes within the basal ganglia: Relevance for the understanding of addiction. Behav. Brain Res. *199*, 89–102.

Berezovskii, V.K., Nassi, J.J., and Born, R.T. (2011). Segregation of feedforward and feedback projections in mouse visual cortex. J. Comp. Neurol. *519*, 3672–3683.

Binzegger, T., Douglas, R.J., and Martin, K. a C. (2004). A quantitative map of the circuit of cat primary visual cortex. J. Neurosci. *24*, 8441–8453.

Binzegger, T., Douglas, R.J., and Martin, K.A.C. (2007). Stereotypical bouton clustering of individual neurons in cat primary visual cortex. J. Neurosci. *27*, 12242–12254.

Bogacz, R. (2020). Dopamine role in learning and action inference. Elife *9*.

Bottjer, S.W., Miesner, E.A., and Arnold, A.P. (1984). Forebrain lesions disrupt development but not maintenance of song in passerine birds. Science (80-.). *224*, 901–903.

Brainard, M.S., and Doupe, A.J. (2000). Auditory feedback in learning and maintenance of vocal behaviour. Nat. Rev. Neurosci. *1*, 31–40.

Burke, D.A., Rotstein, H.G., and Alvarez, V.A. (2017). Striatal Local Circuitry: A New Framework for Lateral Inhibition. Neuron *96*, 267–284.

Callaway, E.M. (2004). Feedforward, feedback and inhibitory connections in primate visual cortex. Neural Networks *17*, 625–632.

Callaway, E.M., and Luo, L. (2015). Monosynaptic circuit tracing with glycoprotein-deleted rabies viruses. J. Neurosci. *35*, 8979–8985.

Carr, D.B., and Sesack, S.R. (1998). Callosal terminals in the rat prefrontal cortex: synaptic targets and association with GABA-immunoreactive structures. Synapse *29*, 193–205.

Carrasco, A., Brown, T.A., Kok, M.A., Chabot, N., Kral, A., and Lomber, S.G. (2013). Influence of core auditory cortical areas on acoustically evoked activity in contralateral primary auditory cortex. J. Neurosci. *33*, 776–789.

Castañé Anna, A., Theobald, D.E.H., and Robbins, T.W. (2010). Selective lesions of the dorsomedial striatum impair serial spatial reversal learning in rats. Behav. Brain Res. *210*, 74–83.

Cauli, B., Zhou, X., Tricoire, L., Toussay, X., and Staiger, J.F. (2014). Revisiting enigmatic cortical calretinin-expressing interneurons. Front. Neuroanat. *8*.

Cerri, C., Restani, L., and Caleo, M. (2010). Callosal contribution to ocular dominance in rat primary visual cortex. Eur. J. Neurosci. *32*, 1163–1169.

Chatterjee, S., Sullivan, H.A., MacLennan, B.J., Xu, R., Hou, Y., Lavin, T.K., Lea, N.E., Michalski, J.E., Babcock, K.R., Dietrich, S., et al. (2018). Nontoxic, double-deletion-mutant rabies viral vectors for retrograde targeting of projection neurons. Nat. Neurosci. *21*, 638–646.

Chen, T.W., Wardill, T.J., Sun, Y., Pulver, S.R., Renninger, S.L., Baohan, A., Schreiter, E.R., Kerr, R.A., Orger, M.B., Jayaraman, V., et al. (2013). Ultrasensitive fluorescent

proteins for imaging neuronal activity. Nature *499*, 295–300.

Cissé, Y., Cissé, C., Grenier, O., Timofeev, I., and Steriade, M. (2003). Electrophysiological Properties and Input-Output Organization of Callosal Neurons in Cat Association Cortex.

Cissé, Y., Nita, D.A., Steriade, M., and Timofeev, I. (2007). Callosal responses of fast-rhythmic-bursting neurons during slow oscillation in cats. Neuroscience *147*, 272–276.

Constantinople, C.M., and Bruno, R.M. (2013). Deep cortical layers are activated directly by thalamus. Science (80-.). *340*, 1591–1594.

da Costa, N.M., and Martin, K.A.C. (2009). The Proportion of Synapses Formed by the Axons of the Lateral Geniculate Nucleus in Layer 4 of Area 17 of the Cat. J. Comp. Neurol. *276*, 264–276.

da Costa, N.M., and Martin, K.A.C. (2010). Whose cortical column would that be? Front. Neuroanat. *4*, 16.

Da Costa, N.M., and Martin, K.A.C. (2011). How thalamus connects to spiny stellate cells in the cat's visual cortex. J. Neurosci. *31*, 2925–2937.

Cui, G., Jun, S.B., Jin, X., Pham, M.D., Vogel, S.S., Lovinger, D.M., and Costa, R.M. (2013). Concurrent activation of striatal direct and indirect pathways during action initiation. Nature *494*, 238–242.

D'souza, R.D., Wang, Q., Ji, W., Meier, A.M., Kennedy, H., Knoblauch, K., and Burkhalter, A. (2020). Canonical and noncanonical features of the mouse visual cortical hierarchy. BioRxiv 2020.03.30.016303.

D'Souza, R.D., and Burkhalter, A. (2017). A laminar organization for selective cortico-cortical communication. Front. Neuroanat. *11*, 71.

D'Souza, R.D., Meier, A.M., Bista, P., Wang, Q., and Burkhalter, A. (2016). Recruitment of inhibition and excitation across mouse visual cortex depends on the hierarchy of interconnecting areas. Elife *5*.

Darian-Smith, C., and Gilbert, C.D. (1994). Axonal sprouting accompanies functional reorganization in adult cat striate cortex. Nature *368*, 737–740.

Denardo, L.A., Berns, D.S., Deloach, K., and Luo, L. (2015). Connectivity of mouse somatosensory and prefrontal cortex examined with trans-synaptic tracing. Nat. Neurosci. *18*, 1687–1697.

Dickinson, A. (1985). Actions and habits: the development of behavioural autonomy. Philos. Trans. R. Soc. London. B, Biol. Sci. *308*, 67–78.

Dombeck, D.A., Khabbaz, A.N., Collman, F., Adelman, T.L., and Tank, D.W. (2007). Imaging Large-Scale Neural Activity with Cellular Resolution in Awake, Mobile Mice. Neuron *56*, 43–57.

Douglas, R.J., and Martin, K.A. (1991). A functional microcircuit for cat visual cortex. J. Physiol. *440*, 735–769.

Douglas, R.J., and Martin, K.A.C. (2004). Neuronal Circuits of the Neocortex. Annu. Rev. Neurosci. *27*, 419–451.

Douglas, R.J., Martin, K.A.C., and Whitteridge, D. (1989). A Canonical Microcircuit for Neocortex. Neural Comput. *1*, 480–488.

Ercsey-Ravasz, M., Markov, N.T., Lamy, C., VanEssen, D.C., Knoblauch, K., Toroczkai, Z., and Kennedy, H. (2013). A Predictive Network Model of Cerebral Cortical Connectivity Based on a Distance Rule. Neuron *80*, 184–197.

Fairént, A., Regidort, J., and Kruger, L. (1992). The cerebral cortex of the mouse (a first contribution-the "acoustic" cortex). Somatosens. Mot. Res. *9*, 3–36.

Fame, R.M., MacDonald, J.L., and Macklis, J.D. (2011). Development, specification, and diversity of callosal projection neurons. Trends Neurosci. *34*, 41–50.

Fee, M.S., and Goldberg, J.H. (2011). A hypothesis for basal ganglia-dependent reinforcement learning in the songbird. Neuroscience *198*, 152–170.

Finlay, B.L. (2016). Principles of Network Architecture Emerging from Comparisons of the Cerebral Cortex in Large and Small Brains. PLoS Biol. *14*, e1002556.

Fino, E., and Yuste, R. (2011). Dense inhibitory connectivity in neocortex. Neuron *69*, 1188–1203.

Fischer, K.B., Collins, H.K., and Callaway, E.M. (2019). Sources of off-target expression from recombinasedependent AAV vectors and mitigation with cross-over insensitive ATG-out vectors. Proc. Natl. Acad. Sci. U. S. A. *116*, 27001–27010.

Fiser, A., Mahringer, D., Oyibo, H.K., Petersen, A. V., Leinweber, M., and Keller, G.B. (2016). Experience-dependent spatial expectations in mouse visual cortex. Nat. Neurosci. *19*, 1658–1664.

Franklin, K.B.J., and Paxinos, G. (2012). Paxinos and Franklin's The mouse brain in stereotaxic coordinates, 4th Edition. (Elsevier).

Freund, T.F., Martin, K.A.C., Soltesz, I., Somogyi, P., and Whitteridge, D. (1989). Arborisation pattern and postsynaptic targets of physiologically identified thalamocortical afferents in striate cortex of the macaque monkey. J. Comp. Neurol. *289*, 315–336.

Fu, Y., Tucciarone, J.M., Espinosa, J.S., Sheng, N., Darcy, D.P., Nicoll, R.A., Huang, Z.J., and Stryker, M.P. (2014). A cortical circuit for gain control by behavioral state. Cell *156*, 1139–1152.

Gagnon, D., Petryszyn, S., Sanchez, M.G., Bories, C., Beaulieu, J.M., De Koninck, Y., Parent, A., and Parent, M. (2017). Striatal Neurons Expressing D1 and D2 Receptors are Morphologically Distinct and Differently Affected by Dopamine Denervation in Mice. Sci. Rep. *7*.

Gămănuț, R., Kennedy, H., Toroczkai, Z., Ercsey-Ravasz, M., Van Essen, D.C., Knoblauch, K., and Burkhalter, A. (2018). The Mouse Cortical Connectome, Characterized by an Ultra-Dense Cortical Graph, Maintains Specificity by Distinct Connectivity Profiles. Neuron *97*, 698-715.e10.

Gerfen, C.R., Paletzki, R., and Heintz, N. (2013). GENSAT BAC cre-recombinase driver lines to study the functional

organization of cerebral cortical and basal ganglia circuits. Neuron *80*, 1368–1383.

Gerfen, C.R., Economo, M.N., and Chandrashekar, J. (2018). Long Distance Projections of Cortical Pyramidal Neurons HHS Public Access. J Neurosci Res *96*, 1467–1475.

Gilbert, C.D., and Li, W. (2012). Adult Visual Cortical Plasticity. Neuron *75*, 250–264.

Gilbert, C.D., and Li, W. (2013). Top-down influences on visual processing (Nature Publishing Group).

Gilbert, C.D., and Sigman, M. (2007). Brain States: Top-Down Influences in Sensory Processing (Cell Press).

Gilbert, C.D., and Wiesel, T.N. (1979). Morphology and intracortical projections of functionally characterised neurones in the cat visual cortex. Nature *280*, 120–125.

Gonchar, Y., Wang, Q., and Burkhalter, A. (2008). Multiple distinct subtypes of GABAergic neurons in mouse visual cortex identified by triple immunostaining. Front. Neuroanat. *1*, 3.

Gong, S., Doughty, M., Harbaugh, C.R., Cummins, A., Hatten, M.E., Heintz, N., and Gerfen, C.R. (2007). Targeting Cre recombinase to specific neuron populations with bacterial artificial chromosome constructs. J. Neurosci. *27*, 9817–9823.

Graybiel, A.M. (1998). The basal ganglia and chunking of action repertoires. In Neurobiology of Learning and Memory, (Academic Press Inc.), pp. 119–136.

Graybiel, A.M. (2008). Habits, rituals, and the evaluative brain. Annu. Rev. Neurosci. *31*, 359–387.

Greig, L.C., Woodworth, M.B., Galazo, M.J., Padmanabhan, H., and Macklis, J.D. (2013). Molecular logic of neocortical projection neuron specification, development and diversity. Nat. Rev. Neurosci. *14*, 755–769.

Gremel, C.M., and Costa, R.M. (2013). Orbitofrontal and striatal circuits dynamically encode the shift between goal-directed and habitual actions. Nat. Commun. *4*, 1–12.

Hahnloser, R.H.R., Kozhewkoy, A.A., and Fee, M.S. (2002). An ultra-sparse code underlies the generation of neural sequences in a songbird. Nature *419*, 65–69.

Harris, K.D., and Mrsic-Flogel, T.D. (2013). Cortical connectivity and sensory coding. Nature *503*, 51–58.

Harris, K.D., and Shepherd, G.M.G.G. (2015). The neocortical circuit: Themes and variations. Nat. Neurosci. *18*, 170–181.

Harris, J.A., Mihalas, S., Hirokawa, K.E., Whitesell, J.D., Choi, H., Bernard, A., Bohn, P., Caldejon, S., Casal, L., Cho, A., et al. (2019). Hierarchical organization of cortical and thalamic connectivity. Nature *575*, 195–202.

Hegdé, J., and Felleman, D.J. (2007). Reappraising the functional implications of the primate visual anatomical hierarchy. Neuroscientist *13*, 416–421.

Heindorf, M., Arber, S., and Keller, G.B. (2018). Mouse Motor Cortex Coordinates the Behavioral Response to Unpredicted Sensory Feedback. Neuron *99*, 1040-1054.e5.

Helmholtz, H. von (1867). Handbuch der physiologischen Optik.

Herculano-Houzel, S. (2012). The remarkable, yet not extraordinary, human brain as a scaled-up primate brain and its associated cost. Proc. Natl. Acad. Sci. U. S. A. *109*, 10661–10668.

Hikosaka, O., Sakai, K., Lu, X., Nakahara, H., Rand, M.K., Nakamura, K., Miyachi, S., and Doya, K. (1999). Parallel neural networks for learning sequential procedures. Trends Neurosci. *22*, 464–471.

Hikosaka, O., Takikawa, Y., and Kawagoe, R. (2000). Role of the basal ganglia in the control of purposive saccadic eye movements. Physiol. Rev. *80*, 953–978.

Hilario, M., Holloway, T., Jin, X., and Costa, R.M. (2012). Different dorsal striatum circuits mediate action discrimination and action generalization. Eur. J. Neurosci. *35*, 1105–1114.

Hintiryan, H., Foster, N.N., Bowman, I., Bay, M., Song, M.Y., Gou, L., Yamashita, S., Bienkowski, M.S., Zingg, B., Zhu, M., et al. (2016). The mouse cortico-striatal projectome. Nat. Neurosci. *19*, 1100–1114.

Hippenmeyer, S., Vrieseling, E., Sigrist, M., Portmann, T., Laengle, C., Ladle, D.R., and Arber, S. (2005). A Developmental Switch in the Response of DRG Neurons to ETS Transcription Factor Signaling. PLoS Biol. *3*, e159.

Hofer, S.B., Ko, H., Pichler, B., Vogelstein, J., Ros, H., Zeng, H., Lein, E., Lesica, N.A., and Mrsic-Flogel, T.D. (2011). Differential connectivity and response dynamics of excitatory and inhibitory neurons in visual cortex. Nat. Neurosci. *14*.

Van Hooser, S.D. (2007). Similarity and diversity in visual cortex: Is there a unifying theory of cortical computation? Neuroscientist *13*, 639–656.

Horvát, S., Gămănuț, R., Ercsey-Ravasz, M., Magrou, L., Gămănuț, B., Van Essen, D.C., Burkhalter, A., Knoblauch, K., Toroczkai, Z., and Kennedy, H. (2016). Spatial Embedding and Wiring Cost Constrain the Functional Layout of the Cortical Network of Rodents and Primates. PLoS Biol. *14*, e1002512.

Ibrahim, L.A., Mesik, L., Ji, X. ying, Fang, Q., Li, H. fu, Li, Y. tang, Zingg, B., Zhang, L.I., and Tao, H.W. (2016). Cross-Modality Sharpening of Visual Cortical Processing through Layer-1-Mediated Inhibition and Disinhibition. Neuron *89*, 1031–1045.

Iurilli, G., Ghezzi, D., Olcese, U., Lassi, G., Nazzaro, C., Tonini, R., Tucci, V., Benfenati, F., and Medini, P. (2012). Sound-driven synaptic inhibition in primary visual cortex. Neuron *73*, 814–828.

Iwasaki, Y., Ohtani, S., and Clark, H.F. (1975). Maturation of rabies virus by budding from neuronal cell membrane in suckling mouse brain. J. Virol. *15*, 1020–1023.

Kao, M.H., Doupe, A.J., and Brainard, M.S. (2005). Contribution of an avian basal ganglia-forebrain circuit to real-time modulation of song. Nature *433*, 638–643.

Karayannis, T., Huerta-Ocampo, I., and Capogna, M. (2007). GABAergic and Pyramidal Neurons of Deep Cortical Layers Directly Receive and Differently Integrate Callosal Input. Cereb. Cortex *17*, 1213–1226.

Kawaguchi, Y. (1992). Receptor subtypes involved in callosally-induced postsynaptic potentials in rat frontal agranular cortex in vitro. Exp. Brain Res. *88*, 33–40.

Keck, T., Mrsic-Flogel, T.D., Vaz Afonso, M., Eysel, U.T., Bonhoeffer, T., and Hübener, M. (2008). Massive restructuring of neuronal circuits during functional reorganization of adult visual cortex. Nat. Neurosci. *11*, 1162–1167.

Keeler, J.F., Pretsell, D.O., and Robbins, T.W. (2014). Functional implications of dopamine D1 vs. D2 receptors: A "prepare and select" model of the striatal direct vs. indirect pathways. Neuroscience *282*, 156–175.

Keller, G.B., and Hahnloser, R.H.R. (2009). Neural processing of auditory feedback during vocal practice in a songbird. Nature *457*, 187–190.

Keller, G.B., and Mrsic-Flogel, T.D. (2018). Predictive Processing: A Canonical Cortical Computation. Neuron *100*, 424–435.

Keller, G.B., Bonhoeffer, T., and Hübener, M. (2012). Sensorimotor Mismatch Signals in Primary Visual Cortex of the Behaving Mouse. Neuron *74*, 809–815.

Khibnik, L.A., Tritsch, N.X., and Sabatini, B.L. (2014). A Direct Projection from Mouse Primary Visual Cortex to Dorsomedial Striatum. PLoS One *9*, e104501.

Kim, E.J., Juavinett, A.L., Kyubwa, E.M., Jacobs, M.W., and Callaway, E.M. (2015). Three Types of Cortical Layer 5 Neurons That Differ in Brain-wide Connectivity and Function. Neuron *88*, 1253–1267.

Knoblich, U., Huang, L., Zeng, H., and Li, L. (2019). Neuronal cell-subtype specificity of neural synchronization in mouse primary visual cortex. Nat. Commun. *10*, 1–13.

Kravitz, A. V., Freeze, B.S., Parker, P.R.L., Kay, K., Thwin, M.T., Deisseroth, K., and Kreitzer, A.C. (2010). Regulation of parkinsonian motor behaviours by optogenetic control of basal ganglia circuitry. Nature *466*, 622–626.

Kumar, S.S., and Huguenard, J.R. (2001). Properties of excitatory synaptic connections mediated by the corpus callosum in the developing rat neocortex. J. Neurophysiol. *86*, 2973–2985.

Kumar, S.S., and Huguenard, J.R. (2003). Pathway-Specific Differences in Subunit Composition of Synaptic NMDA Receptors on Pyramidal Neurons in Neocortex. J. Neurosci. *23*, 10074–10083.

Latawiec, D., Martin, K.A., and Meskenaite, V. (2000). Termination of the geniculocortical projection in the striate cortex of macaque monkey: a quantitative immunoelectron microscopic study. J. Comp. Neurol. *419*, 306–319.

Leinweber, M., Zmarz, P., Buchmann, P., Argast, P., Hübener, M., Bonhoeffer, T., and Keller, G.B. (2014). Two-photon calcium imaging in mice navigating a virtual reality environment. J. Vis. Exp. e50885.

Leinweber, M., Ward, D.R., Sobczak, J.M., Attinger, A., and Keller, G.B. (2017). A Sensorimotor Circuit in Mouse Cortex for Visual Flow Predictions. Neuron *95*, 1420-1432.e5.

De León Reyes, N.S., Mederos, S., Varela, I., Weiss, L.A., Perea, G., Galazo, M.J., and Nieto, M. (2019). Transient callosal projections of L4 neurons are eliminated for the acquisition of local connectivity. Nat. Commun. *10*, 1–15.

Levene, M.J., Dombeck, D.A., Kasischke, K.A., Molloy, R.P., and Webb, W.W. (2004). In Vivo Multiphoton Microscopy of Deep Brain Tissue. J. Neurophysiol. *91*, 1908–1912.

Luo, M., Ding, L., and Perkel, D.J. (2001). An avian basal ganglia pathway essential for vocal learning forms a closed topographic loop. J. Neurosci. *21*, 6836–6845.

Madisen, L., Zwingman, T.A., Sunkin, S.M., Oh, S.W., Zariwala, H.A., Gu, H., Ng, L.L., Palmiter, R.D., Hawrylycz, M.J., Jones, A.R., et al. (2010). A robust and high-throughput Cre reporting and characterization system for the whole mouse brain. Nat. Neurosci. *13*, 133–140.

Mahringer, D. (2018). Functional correlates of immediate early gene expression in visual cortex and hippocampus. University of Basel.

Markov, N.T., and Kennedy, H. (2013). The importance of being hierarchical. Curr. Opin. Neurobiol. *23*, 187–194.

Markov, N.T., Misery, P., Falchier, A., Lamy, C., Vezoli, J., Quilodran, R., Gariel, M.A., Giroud, P., Ercsey-Ravasz, M., Pilaz, L.J., et al. (2011). Weight consistency specifies regularities of macaque cortical networks. Cereb. Cortex *21*, 1254–1272.

Markov, N.T., Ercsey-Ravasz, M., Lamy, C., Ribeiro Gomes, A.R., Magrou, L., Misery, P., Giroud, P., Barone, P., Dehay, C., Toroczkai, Z., et al. (2013). The role of long-range connections on the specificity of the macaque interareal cortical network. Proc. Natl. Acad. Sci. U. S. A. *110*, 5187–5192.

Markov, N.T., Vezoli, J., Chameau, P., Falchier, A., Quilodran, R., Huissoud, C., Lamy, C., Misery, P., Giroud, P., Ullman, S., et al. (2014a). Anatomy of hierarchy: Feedforward and feedback pathways in macaque visual cortex. J. Comp. Neurol. *522*, 225–259.

Markov, N.T., Ercsey-Ravasz, M.M., Ribeiro Gomes, A.R., Lamy, C., Magrou, L., Vezoli, J., Misery, P., Falchier, A., Quilodran, R., Gariel, M.A., et al. (2014b). A weighted and directed interareal connectivity matrix for macaque cerebral cortex. Cereb. Cortex *24*, 17–36.

Markowitz, J.E., Gillis, W.F., Beron, C.C., Neufeld, S.Q., Robertson, K., Bhagat, N.D., Peterson, R.E., Peterson, E., Hyun, M., Linderman, S.W., et al. (2018). The Striatum Organizes 3D Behavior via Moment-to-Moment Action Selection. Cell *174*, 44-58.e17.

Markram, H., Toledo-Rodriguez, M., Wang, Y., Gupta, A., Silberberg, G., and Wu, C. (2004). Interneurons of the neocortical inhibitory system. Nat. Rev. Neurosci. *5*, 793–807.

Mink, J.W. (1996). The basal ganglia: Focused selection and inhibition of competing motor programs. Prog. Neurobiol. *50*, 381–425.

Mishchenko, Y., Hu, T., Spacek, J., Mendenhall, J., Harris, K.M., and Chklovskii, D.B. (2010). Ultrastructural analysis of hippocampal neuropil from the connectomics perspective. Neuron *67*, 1009–1020.

Miyachi, S., Hikosaka, O., Miyashita, K., Kárádi, Z., and Rand, M.K. (1997). Differential roles of monkey striatum in learning of sequential hand movement. Exp. Brain Res. *115*, 1–5.

Miyachi, S., Hikosaka, O., and Lu, X. (2002). Differential activation of monkey striatal neurons in the early and late stages of procedural learning. Exp. Brain Res. *146*, 122–126.

Miyamichi, K., Shlomai-Fuchs, Y., Shu, M., Weissbourd, B.C., Luo, L., and Mizrahi, A. (2013). Dissecting local circuits: Parvalbumin interneurons underlie broad feedback control of olfactory bulb output. Neuron *80*, 1232–1245.

Mountcastle, V.B. (1957). Modality and topographic properties of single neurons of cat's somatic sensory cortex. J. Neurophysiol. *20*, 408–434.

Mountcastle, V.B. (1997). The columnar organization of the neocortex. Brain *120*, 701–722.

Moussa, R., Poucet, B., Amalric, M., and Sargolini, F. (2011). Contributions of dorsal striatal subregions to spatial alternation behavior. Learn. Mem. *18*, 444–451.

Murphy, K., James, L.S., Sakata, J.T., and Prather, J.F. (2017). Advantages of comparative studies in songbirds to understand the neural basis of sensorimotor integration. J. Neurophysiol. *118*, 800–816.

Neely, R.M., Koralek, A.C., Athalye, V.R., Costa, R.M., and Carmena, J.M. (2018). Volitional Modulation of Primary Visual Cortex Activity Requires the Basal Ganglia. Neuron *97*, 1356-1368.e4.

Nelson, A.B., and Kreitzer, A.C. (2014). Reassessing Models of Basal Ganglia Function and Dysfunction. Annu. Rev. Neurosci. *37*, 117–135.

Niell, C.M. (2015). Cell Types, Circuits, and Receptive Fields in the Mouse Visual Cortex. Annu. Rev. Neurosci. *38*, 413–431.

Niell, C.M., and Stryker, M.P. (2008). Highly selective receptive fields in mouse visual cortex. J. Neurosci. *28*, 7520–7536.

Ölveczky, B.P., Andalman, A.S., and Fee, M.S. (2005). Vocal Experimentation in the Juvenile Songbird Requires a Basal Ganglia Circuit. PLoS Biol. *3*, e153.

Paille, V., Fino, E., Du, K., Morera-Herreras, T., Perez, S., Kotaleski, J.H., and Venance, L. (2013). GABAergic circuits control spike-timing-dependent plasticity. J. Neurosci. *33*, 9353–9363.

Palmer, L.M., Schulz, J.M., Murphy, S.C., Ledergerber, D., Murayama, M., and Larkum, M.E. (2012). The cellular basis of GABAB-mediated interhemispheric inhibition. Science (80-.). *335*, 989–993.

Payne, B.R., Siwek, D.F., and Lomber, S.G. (1991). Complex transcallosal interactions in visual cortex. Vis. Neurosci. *6*, 283–287.

Peters, S.K., Dunlop, K., and Downar, J. (2016). Cortico-striatal-thalamic loop circuits of the salience network: A central pathway in psychiatric disease and treatment. Front. Syst. Neurosci. *10*, 104.

Petreanu, L., Huber, D., Sobczyk, A., and Svoboda, K. (2007). Channelrhodopsin-2-assisted circuit mapping of long-range callosal projections. Nat. Neurosci. *10*, 663–668.

Pfeffer, C.K., Xue, M., He, M., Huang, Z.J., and Scanziani, M. (2013). Inhibition of inhibition in visual cortex: The logic of connections between molecularly distinct interneurons. Nat. Neurosci. *16*, 1068–1076.

Powell, A., Connelly, W.M., Vasalauskaite, A., Nelson, A.J.D., Vann, S.D., Aggleton, J.P., Sengpiel, F., and Ranson, A. (2020). Stable Encoding of Visual Cues in the Mouse Retrosplenial Cortex. Cereb. Cortex.

Quiquempoix, M., Fayad, S.L., Boutourlinsky, K., Leresche, N., Gis, R., Lambert, C., and Correspondence, T.B. (2018). Layer 2/3 Pyramidal Neurons Control the Gain of Cortical Output.

Ragozzino, M.E., Ragozzino, K.E., Mizumori, S.J.Y., and Kesner, R.P. (2002). Role of the dorsomedial striatum in behavioral flexibility for response and visual cue discrimination learning. Behav. Neurosci. *116*, 105–115.

Reardon, T.R., Murray, A.J., Turi, G.F., Wirblich, C., Croce, K.R., Schnell, M.J., Jessell, T.M., and Losonczy, A. (2016). Rabies Virus CVS-N2cδG Strain Enhances Retrograde Synaptic Transfer and Neuronal Viability. Neuron *89*, 711–724.

Reig, R., and Silberberg, G. (2014). Multisensory Integration in the Mouse Striatum. Neuron *83*, 1200–1212.

Reiner, A., Medina, L., and Veenman, C.L. (1998). Structural and functional evolution of the basal ganglia in vertebrates. Brain Res. Rev. *28*, 235–285.

Restani, L., Cerri, C., Pietrasanta, M., Gianfranceschi, L., Maffei, L., and Caleo, M. (2009). Functional Masking of Deprived Eye Responses by Callosal Input during Ocular Dominance Plasticity. Neuron *64*, 707–718.

Rock, C., and Apicella, A. (2015). Callosal projections drive neuronal-specific responses in the mouse auditory cortex. J. Neurosci. *35*, 6703–6713.

Rossi, L.F., Harris, K., and Carandini, M. (2019). Excitatory and inhibitory intracortical circuits for orientation and direction selectivity. BioRxiv 556795.

Roth, M.M., Dahmen, J.C., Muir, D.R., Imhof, F., Martini, F.J., and Hofer, S.B. (2016). Thalamic nuclei convey diverse contextual information to layer 1 of visual cortex. Nat. Neurosci. *19*, 299–307.

Ruigrok, T.J.H., van Touw, S., and Coulon, P. (2016). Caveats in transneuronal tracing with unmodified rabies virus: An evaluation of aberrant results using a nearly perfect tracing technique. Front. Neural Circuits *10*.

Saleem, A.B., Diamanti, E.M., Fournier, J., Harris, K.D., and Carandini, M. (2018). Coherent encoding of subjective spatial position in visual cortex and hippocampus. Nature *562*, 124–127.

Sato, T.K., Häusser, M., and Carandini, M. (2014). Distal connectivity causes summation and division across mouse visual cortex. Nat. Neurosci. *17*, 30–32.

Scharff, C., and Nottebohm, F. (1991). A comparative study of the behavioral deficits following lesions of various parts of the zebra finch song system: Implications for vocal learning. J. Neurosci. *11*, 2896–2913.

Schultz, W. (2013). Updating dopamine reward signals. Curr. Opin. Neurobiol. *23*, 229–238.

Sempere-Ferràndez, A., Andrés-Bayón, B., and Geijo-Barrientos, E. (2018). Callosal responses in a retrosplenial column. Brain Struct. Funct. *223*, 1051–1069.

Shen, W., Flajolet, M., Greengard, P., and Surmeier, D.J. (2008). Dichotomous dopaminergic control of striatal synaptic plasticity. Science (80-.). *321*, 848–851.

Shin, J.H., Kim, D., and Jung, M.W. (2018). Differential coding of reward and movement information in the dorsomedial striatal direct and indirect pathways. Nat. Commun. *9*, 1–14.

Shipp, S. (2017). The functional logic of corticostriatal connections. Brain Struct. Funct. *222*, 669–706.

Smith, K.S., and Graybiel, A.M. (2013). A dual operator view of habitual behavior reflecting cortical and striatal dynamics. Neuron *79*, 361–374.

Stephenson-Jones, M., Ericsson, J., Robertson, B., and Grillner, S. (2012). Evolution of the basal ganglia: Dual-output pathways conserved throughout vertebrate phylogeny. J. Comp. Neurol. *520*, 2957–2973.

Taniguchi, H., He, M., Wu, P., Kim, S., Paik, R., Sugino, K., Kvitsani, D., Fu, Y., Lu, J., Lin, Y., et al. (2011). A Resource of Cre Driver Lines for Genetic Targeting of GABAergic Neurons in Cerebral Cortex. Neuron *71*, 995–1013.

Tecuapetla, F., Jin, X., Lima, S.Q., and Costa, R.M. (2016). Complementary Contributions of Striatal Projection Pathways to Action Initiation and Execution. Cell *166*, 703–715.

Tervo, D.G.R., Hwang, B.-Y., Viswanathan, S., Gaj, T., Lavzin, M., Ritola, K.D., Lindo, S., Michael, S., Kuleshova, E., Ojala, D., et al. (2016). A Designer AAV Variant Permits Efficient Retrograde Access to Projection Neurons. Neuron *92*, 372–382.

Toldi, J., Wolff, J.R., and Wiese, U.H. (1989). Functional consequences of modification of callosal connections by perinatal enucleation in rat visual cortex. Neuroscience *33*, 517–524.

Troyer, T.W., and Bottjer, S.W. (2001). Birdsong: Models and mechanisms. Curr. Opin. Neurobiol. *11*, 721–726.

Ugolini, G. (1995). Specificity of rabies virus as a transneuronal tracer of motor networks: Transfer from hypoglossal motoneurons to connected second-order and higher order central nervous system cell groups. J. Comp. Neurol. *356*, 457–480.

Velasco, M.G.M., and Levene, M.J. (2014). In vivo two-photon microscopy of the hippocampus using glass plugs. Biomed. Opt. Express *5*, 1700.

Vélez-Fort, M., Bracey, E.F., Keshavarzi, S., Rousseau, C. V, Cossell, L., Lenzi, S.C., Strom, M., and Margrie, T.W. (2018). A Circuit for Integration of Head- and Visual-Motion Signals in Layer 6 of Mouse Primary Visual Cortex. Neuron *98*, 179-191.e6.

Vogt, B.A., and Gorman, A.L.F. (1982). Responses of cortical neurons to stimulation of corpus callosum in vitro. J. Neurophysiol. *48*, 1257–1273.

Wang, Q., and Burkhalter, A. (2007). Area map of mouse visual cortex. J. Comp. Neurol. *502*, 339–357.

Wang, X.J., and Kennedy, H. (2016). Brain structure and dynamics across scales: In search of rules. Curr. Opin. Neurobiol. *37*, 92–98.

Wang, L., Rangarajan, K. V., Gerfen, C.R., and Krauzlis, R.J. (2018). Activation of Striatal Neurons Causes a Perceptual Decision Bias during Visual Change Detection in Mice. Neuron *97*, 1369-1381.e5.

Wang, Q., Sporns, O., and Burkhalter, A. (2012). Network analysis of corticocortical connections reveals ventral and dorsal processing streams in mouse visual cortex. J. Neurosci. *32*, 4386–4399.

Wertz, A., Trenholm, S., Yonehara, K., Hillier, D., Raics, Z., Leinweber, M., Szalay, G., Ghanem, A., Keller, G., Rozsa, B., et al. (2015). Single-cell-initiated monosynaptic tracing reveals layer-specific cortical network modules. Science (80-.). *349*, 70–74.

Wickersham, I.R., Lyon, D.C., Barnard, R.J.O.O., Mori, T., Finke, S., Conzelmann, K.-K.K., Young, J.A.T.T., and Callaway, E.M. (2007a). Monosynaptic Restriction of Transsynaptic Tracing from Single, Genetically Targeted Neurons. Neuron *53*, 639–647.

Wickersham, I.R., Finke, S., Conzelmann, K.K., and Callaway, E.M. (2007b). Retrograde neuronal tracing with a deletion-mutant rabies virus. Nat. Methods *4*, 47–49.

Wickersham, I.R., Sullivan, H.A., and Seung, H.S. (2010). Production of glycoprotein-deleted rabies viruses for monosynaptic tracing and high-level gene expression in neurons. Nat. Protoc. *5*, 595–606.

Wolpert, D.M., Diedrichsen, J., and Flanagan, J.R. (2011). Principles of sensorimotor learning. Nat. Rev. Neurosci. *12*, 739–751.

Wood, K.C., Blackwell, J.M., and Geffen, M.N. (2017). Cortical inhibitory interneurons control sensory processing. Curr. Opin. Neurobiol. *46*, 200–207.

Xu, X., Roby, K.D., and Callaway, E.M. (2010). Immunochemical characterization of inhibitory mouse cortical neurons: Three chemically distinct classes of inhibitory cells. J. Comp. Neurol. *518*, 389–404.

Xu, X., Olivas, N.D., Ikrar, T., Peng, T., Holmes, T.C., Nie, Q., and Shi, Y. (2016). Primary visual cortex shows laminar-

specific and balanced circuit organization of excitatory and inhibitory synaptic connectivity. J. Physiol. *594*, 1891–1910.

Yamahachi, H., Marik, S.A., McManus, J.N.J., Denk, W., and Gilbert, C.D. (2009). Rapid Axonal Sprouting and Pruning Accompany Functional Reorganization in Primary Visual Cortex. Neuron *64*, 719–729.

Yamawaki, N., Borges, K., Suter, B.A., Harris, K.D., and Shepherd, G.M.G. (2014). A genuine layer 4 in motor cortex with prototypical synaptic circuit connectivity. Elife *3*, e05422.

Yang, W., Carrasquillo, Y., Hooks, B.M.B.M., Nerbonne, J.M.J.M., and Burkhalter, A. (2013). Distinct Balance of Excitation and Inhibition in an Interareal Feedforward and Feedback Circuit of Mouse Visual Cortex. J. Neurosci. *33*, 17373–17384.

Yanike, M., and Ferrera, V.P. (2014). Representation of outcome risk and action in the anterior caudate nucleus. J. Neurosci. *34*, 3279–3290.

Yin, H.H. (2010). The sensorimotor striatum is necessary for serial order learning. J. Neurosci. *30*, 14719–14723.

Yin, H.H., and Knowlton, B.J. (2006). The role of the basal ganglia in habit formation. Nat. Rev. Neurosci. *7*, 464–476.

Yin, H.H., Knowlton, B.J., and Balleine, B.W. (2004). Lesions of dorsolateral striatum preserve outcome expectancy but disrupt habit formation in instrumental learning. Eur. J. Neurosci. *19*, 181–189.

Zampieri, N., Jessell, T.M., and Murray, A.J. (2014). Mapping sensory circuits by anterograde transsynaptic transfer of recombinant rabies virus. Neuron *81*, 766–778.

Zhang, S., Xu, M., Kamigaki, T., Hoang Do, J.P., Chang, W.-C.C., Jenvay, S., Miyamichi, K., Luo, L., Dan, Y., Do, J.P.H., et al. (2014). Long-range and local circuits for top-down modulation of visual cortex processing. Science (80-.). *345*, 660–665.

Zhang, Y., Jiang, S., Xu, Z., Gong, H., Li, A., Luo, Q., Ren, M., Li, X., Wu, H., Yuan, J., et al. (2019). Pinpointing morphology and projection of excitatory neurons in mouse visual cortex. Front. Neurosci. *13*, 912.

Zhao, X., Liu, M., and Cang, J. (2013). Sublinear binocular integration preserves orientation selectivity in mouse visual cortex. Nat. Commun. *4*.

Zmarz, P., and Keller, G.B. (2016). Mismatch Receptive Fields in Mouse Visual Cortex. Neuron *92*, 766–772.

Znamenskiy, P., Kim, M.-H., Muir, D.R., Iacaruso, M.F., Hofer, S.B., and Mrsic-Flogel, T.D. (2018). Functional selectivity and specific connectivity of inhibitory neurons in primary visual cortex. BioRxiv 294835.